Multispectral confocal 3D imaging of intact healthy and tumor tissue using mLSR-3D

Ineveld, R.L. van; Collot, R.; Roman, M.B.; Pagliaro, A.; Bessler, N.; Ariese, H.C.R.; ... ; Rios, A.C.

nature protocols

PROTOCOL

https://doi.org/10.1038/s41596-022-00739-x

Check for updates

Multispectral confocal 3D imaging of intact healthy and tumor tissue using mLSR-3D

Ravian L. van Ineveld[1,2,6], Raphaël Collot[1,2,6], Mario Barrera Román[1,2], Anna Pagliaro[1,2], Nils Bessler[1,2], Hendrikus C. R. Ariese[1,2], Michiel Kleinnijenhuis[1,2], Marcel Kool[1,3,4], Maria Alieva[1,2], Susana M. Chuva de Sousa Lopes[5], Ellen J. Wehrens[1,2] and Anne C. Rios[1,2]✉

Revealing the 3D composition of intact tissue specimens is essential for understanding cell and organ biology in health and disease. State-of-the-art 3D microscopy techniques aim to capture tissue volumes on an ever-increasing scale, while also retaining sufficient resolution for single-cell analysis. Furthermore, spatial profiling through multi-marker imaging is fast developing, providing more context and better distinction between cell types. Following these lines of technological advance, we here present a protocol based on FUnGI (fructose, urea and glycerol clearing solution for imaging) optical clearing of tissue before multispectral large-scale single-cell resolution 3D (mLSR-3D) imaging, which implements 'on-the-fly' linear unmixing of up to eight fluorophores during a single acquisition. Our protocol removes the need for repetitive illumination, thereby allowing larger volumes to be scanned with better image quality in less time, also reducing photo-bleaching and file size. To aid in the design of multiplex antibody panels, we provide a fast and manageable intensity equalization assay with automated analysis to design a combination of markers with balanced intensities suitable for mLSR-3D. We demonstrate effective mLSR-3D imaging of various tissues, including patient-derived organoids and xenografted tumors, and, furthermore, describe an optimized workflow for mLSR-3D imaging of formalin-fixed paraffin-embedded samples. Finally, we provide essential steps for 3D image data processing, including shading correction that does not require pre-acquired shading references and 3D inhomogeneity correction to correct fluorescence artefacts often afflicting 3D datasets. Together, this provides a one-week protocol for eight-fluorescent-marker 3D visualization and exploration of intact tissue of various origins at single-cell resolution.

Introduction

Tissues consist of many different types of intertwined cells with various shapes that are intricately organized in three dimensions. The interactions and relationships between these cells are crucial for their function, and therefore unraveling the cellular composition of tissues is essential. By visualizing cells in their 3D environment, we can fully appreciate the significance of their localization, interconnection and morphology. This spatio-phenotypic profiling of biological specimens aims to—in a single overview—capture the expressed traits of diverse cell types on which normal tissue function depends and how this is altered in pathological settings like cancer. As such, 3D imaging has provided critical insights into embryonic[1] and organ development[2–4], brain connectivity and function[5], cancer progression[6,7] and cellular cross-talk in the tumor microenvironment[8].

Development of the protocol and comparison with other methods

Non-toxic rapid clearing using fructose, urea and glycerol clearing solution for imaging (FUnGI)

Intact tissues contain various cellular and extracellular components of diverging light refractive indexes, which present a major challenge for volumetric imaging because of profound light scattering[9,10]. Therefore, optical clearing is often required to reduce these differences in refractive indexes, allowing light penetration deep within the tissue. To date, numerous protocols[10–17] have been developed for 3D imaging of intact tissues and 3D tissue models, such as organoids. Each of these methods has their own specific advantages and disadvantages with respect to organ specificity, transparency, antibody compatibility and retention of native fluorescence. In general, solvent-based

[1]Princess Máxima Center for Pediatric Oncology, Utrecht, the Netherlands. [2]Oncode Institute, Utrecht, the Netherlands. [3]Hopp Children's Cancer Center (KiTZ), Heidelberg, Germany. [4]Division of Pediatric Neurooncology, German Cancer Research Center DKFZ and German Cancer Consortium DKTK, Heidelberg, Germany. [5]Department of Anatomy and Embryology, Leiden University Medical Center, Leiden, the Netherlands. [6]These authors contributed equally: Ravian L. van Ineveld, Raphaël Collot. ✉e-mail: a.c.rios@prinsesmaximacentrum.nl

Box 1 | Tissue preparation ● Timing 1 d

Tissue harvesting and preparation for mLSR-3D can vary significantly depending on the origin and size. The following steps apply to mouse brain tissue preparation. To prepare human tissue samples, skip to step 3 below. Organoids of significant size (≥500 µm; e.g., brain organoids) should be processed like large tissue and sectioned by using a vibratome (step 4). For smaller, matrix-embedded organoids, follow the steps described by Dekkers et al.[12] under 'Organoid recovery from 3D matrix' and 'Fixation and blocking' and continue at Step 3 of Procedure 1. For FFPE tissue, prepare as described in Box 3 and continue at step 4 for bigger samples requiring additional sectioning or proceed with the equalization assay (Procedure 1, Step 1) or the main mLSR3D protocol (Procedure 2, Step 1) if the sample is smaller than 500 µm.

1 Euthanize the mouse by using CO_2 and confirm death by respiratory arrest and lack of pedal withdrawal reflex. Perform transcardial perfusion under a fume hood. Cut through the rib cage on either side of the sternum and fold back the sternum to expose the heart. Using a 26-gauge needle, manually inject 10 ml of PBS into the left ventricle (10 ml/min), while creating a small incision in the liver. Liver decolorization is used as an indicator of successful perfusion. Repeat the injection with 10 ml of 4% (wt/vol) PFA pH 7.4 (10 ml/min).
! CAUTION PFA is a toxic substance if swallowed or inhaled or if it comes in contact with skin. Use under a fume hood and wear rubber gloves, protective eye goggles and a laboratory coat.

2 Carefully dissect the brain by using forceps and scissors and separate both hemispheres by using a scalpel.

3 Fix the tissue in a 15-ml tube containing 10 ml of ice cold 4% (wt/vol) PFA pH 7.4. Place the tube on a roller bank at 4 °C.
▲ CRITICAL STEP Fixation time is dependent on the tissue size or origin and ranges from 2 h for fragile embryonic tissue to overnight for large mouse brain or tumor samples.

4 Mix 4% (wt/vol) agarose powder in 20 ml of PBS in a glass beaker. Carefully heat the solution by using a microwave until the agarose is completely dissolved. Avoid boiling of the solution and ensure that no excessive air bubbles are introduced. Let the agarose (4% (wt/vol) in PBS) cool down to 37–40 °C before further use.

5 Embed the tissue in agarose gel (4% (wt/vol) in PBS) by using a mold and cut thick sagittal sections (300–400 µm) with a vibrating blade microtome set at a velocity of 0.6 mm/s, amplitude of 0.9 mm and an angle of 18°.
■ PAUSE POINT Tissue can be stored in PBT at 4 °C for ≤2 d. However, fresh tissue performs best, and the protocol should be continued as soon as possible.

clearing removes water and lipids and typically achieves the best optical transparency[9,18]. However, this often impairs immunolabeling (due to epitope deterioration) or the use of native fluorescent proteins and can lead to tissue deformations[9,19]. In addition, these organic solvents can be toxic, neccessating protective labwear and safety procedures, and protocols can take up to a few weeks[20].

Next to these solvent-based clearing protocols, an increased number of sample preparation methods have been developed specifically tailored to preserving endogenous fluorescence and tissue architecture[7,11,21], performing large sample immunolabeling[17,22] and moving toward multiplex imaging[23–27]. This allowed rapid 3D imaging in various applications, ranging from fluorescently engineered animal models to studying biological processes in human samples. As part of our original large-scale single-cell resolution 3D pipeline, we developed FUnGI[7], an aqueous-based clearing agent used in our protocol. This provides gentle, yet sufficient optical clearing that preserves both tissue architecture and cell morphology, with the advantage of being reversible if the tissue needs to be restained with additional antibodies. FUnGI is compatible with both endogenous fluorescence and immunostaining, and samples can be stored long term (≤6 months) with minimal loss of fluorescence. In addition, FUnGI does not contain toxic components, and the clearing takes only up to 1 d, thereby offering uncomplicated, routine application. This agent has previously been used to clear various tissues, including pediatric spinal ependymoma[26], breast cancer[7] and Wilms tumor[26] and their healthy counterparts, demonstrating the wide-spread application of FUnGI-based 3D imaging. Tissue harvesting and preparation for these applications of multispectral large-scale single-cell resolution 3D (mLSR-3D) can vary significantly depending on the origin and size (Box 1).

Multispectral single-acquisition eight-color 3D imaging

Microscopy has traditionally been limited to acquiring four or five fluorophores at a time, thereby avoiding overlapping emission spectra. However, this provides only a modest phenotypic-resolving capacity. Multiplexing[25,28,29], through sequential rounds of labeling and acquisition, has been successfully used to increase the number of markers that can be imaged in a single sample. However, these approaches become increasingly time consuming and complicated when applied to larger intact 3D tissues, because they require precise co-registration to overlay the datasets and correct for deformation between acquisition rounds. Therefore, alternate strategies aim to increase the number of fluorophores that can be distinguished in a single experiment through post-acquisition compensation of overlapping, yet spectrally resolvable fluorescent signals[21,30,31].

We further advanced these approaches into mLSR-3D imaging, by implementing 'on-the-fly' linear unmixing of up to eight spectrally resolved, yet highly overlapping, fluorophores during acquisition with a multispectral detector[26] (Fig. 1). Thereby, using a linear unmixing algorithm on a

Protocol mLSR-3D

Experimental preparation

Tissue preparation and fixation

Box 1 (Steps 1–5)

Equalization assay

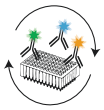

High-throughput single-stainings

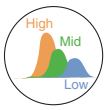

Intensity classification

Optimization of antibody combinations

Procedure 1 (Steps 1–23)

Spectral reference library

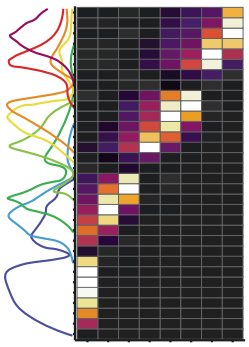

Procedure 1 (Steps 13–14)

Immunostaining

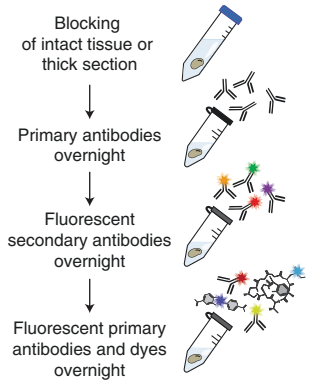

Procedure 2 (Steps 1–8)

FUnGI optical clearing

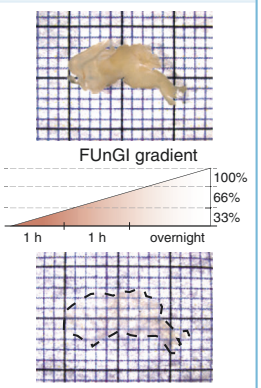

Procedure 2 (Steps 9–12)

3D imaging and preprocessing

3D spectral imaging

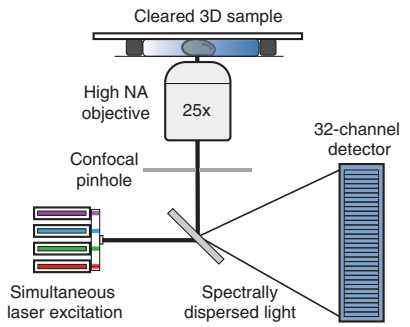

Procedure 2 (Steps 13–19)

Shading correction

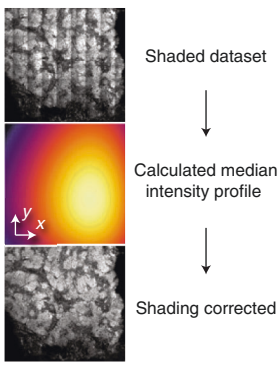

Procedure 2 (Steps 20–24)

3D inhomogeneity correction

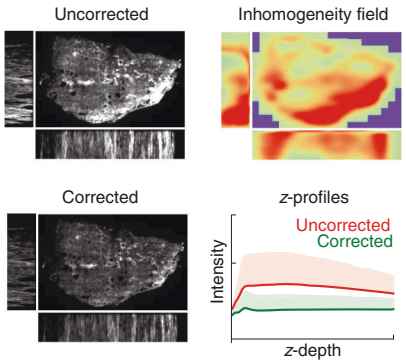

Procedure 2 (Step 25)

Applications of mLSR-3D

3D tissue exploration

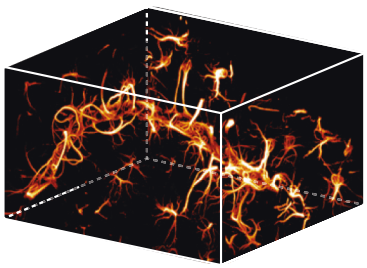

3D single-cell segmentation

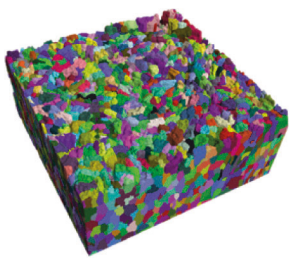

Morphometric and marker analysis

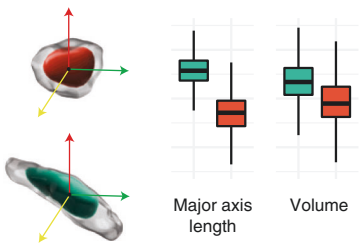

Spatio-phenotypic patterning of healthy and tumor tissues

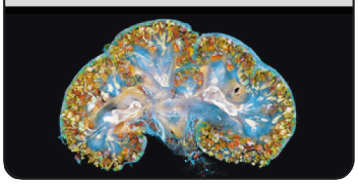

Tumor cell migration in xenograft models

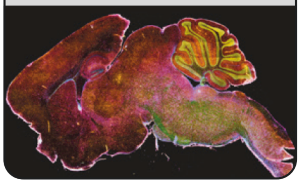

Phenotypic characterization of heterogeneous organoids

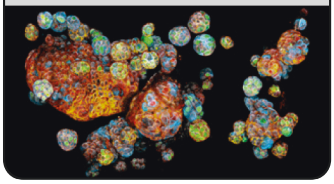

3D phenotyping of archival FFPE tissue

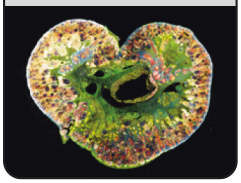

◀ **Fig. 1 | Schematic summary of the mLSR-3D imaging protocol and envisioned applications.** Experimental preparation consists of an equalization assay to assist eight-color mix design, acquisition of a spectral signature reference library for linear unmixing, immunostaining of the tissue and optical clearing by FUnGI. 3D spectral imaging uses simultaneous laser excitation (405, 488, 561 and 633 nm) to excite all fluorophores, and emission is detected by a 32-channel spectral detector. Acquired datasets are shading-corrected by calculating shading profiles and 3D inhomogeneity correction from the STAPL-3D (SegmenTation Analysis by ParaLlelization of 3D Datasets) toolbox to achieve optimal quality in all dimensions. The datasets resulting from the mLSR-3D protocol can be explored in 3D, single-cell segmented and analyzed for morphometrics and marker expression. The protocol is suited for a range of applications, including spatio-phenotypic patterning of tissues, visualizing tumor cell migration, characterization of organoids and 3D phenotyping of archival formalin fixed paraffin-embedded (FFPE) tissue. NA, numerical aperture.

lambda stack, the spectral profiles of every pixel in the image are determined during acquisition, and each fluorophore is separately reassigned to this volume[32] (http://zeiss-campus.magnet.fsu.edu/articles/spectralimaging/introduction.html). Unmixing during acquistion removes the need to store and process large 32-channel lambda files, thereby saving time and storage space.

We optimized our protocol for imaging on a Zeiss LSM 880 confocal microscope equipped with a spectral 32-channel detector. A single voltage setting thereby regulates the overall sensitivity of the detector and cannot be adjusted independently per subchannel. In addition, spectrally adjacent fluorophores can be excited by the same laser line. Therefore, as a prerequisite for mLSR-3D, emission signals should not differ by more than one order of magnitude. This is increasingly challenging to achieve the more antibody combinations are used together. To aid in our single-acquisition, eight-color imaging setup, we developed a workflow for spectral mix design (Extended Data Fig. 1 and Box 2) with commercially available antibodies (Table 1). This relies on a fast and manageable equalization assay, in which the intensity of every primary and secondary antibody available and/or required for the setup of an mLSR-3D experiment is quantified through our high-throughput, automated analysis. This provides in a single overview the quantified intensities of all the available antibodies and dyes. Combinations of fluorescent markers with balanced fluorescent intensities can thereby be easily selected (Fig. 2).

Although the equalization assay requires time and resources to carry out initially, it is still quicker, more efficient and less discouraging than evaluating combinations one at a time. In addition, calibrating the laser output powers by using a laser power meter allows new antibodies and dyes to be added at any time without the need to redo the already established assay. Moreover, the equalization assay provides a practical opportunity to collect the spectral signatures of every fluorophore in a reference library, which needs to be acquired only once. Finally, the obtained results can serve as positive controls that verify that any negative results obtained with an eight-color spectral mix are valid.

Overview of the procedure

The mLSR-3D imaging protocol consist of two procedures covering the key steps for successful multispectral volumetric imaging (Fig. 1). In Procedure 1, we describe our intensity equalization assay, which provides a platform for multispectral mix design (Fig. 2, Box 2 and Extended Data Fig. 2). This consists of tissue preparation (Box 1; Procedure 1, Steps 1 and 2), high-throughput single staining for all relevant primary and secondary antibodies (Procedure 1, Steps 3–8), optical clearing with FUnGI solution (Procedure 1, Steps 9–12), acquisition of a library containing the spectral reference signatures for all fluorophores (Procedure 1, Steps 13 and 14) and reproducible imaging of all primary and secondary antibodies and dyes (Procedure 1, Steps 15–19) followed by automated quantification of their intensities, carried out by using the STAPL-3D (SegmenTation Analysis by ParaLlelization of 3D Datasets) toolbox (Procedure 1, Steps 20–23).

In Procedure 2, we describe the steps required for multispectral imaging of large samples from various sources. This consists of immunostaining of 3D tissue (Procedure 2, Steps 1–8) by using antibody combinations selected on the basis of the equalization assay (see Procedure 1), followed by optical clearing with FUnGI solution (Procedure 2, Steps 9–12). Samples can be kept in FUnGI to pause the protocol or for long-term storage (Procedure 2, Step 12). After sample mounting (Procedure 2, Steps 13–17), intact tissues are imaged by multispectral volumetric imaging (Procedure 2, Steps 18 and 19).

To ensure that all users can perform 3D tissue exploration with optimal quality by using our protocol, we provide optional stepwise 3D image data processing instructions from our STAPL-3D toolbox[26]. This includes details on how to implement a tile shading-correction tool to adjust intensity inconsistencies, typically seen on tile edges. As opposed to conventional shading-correction tools,

Box 2 | Eight-color-mix design walkthrough example

This box describes the thought process for the design of an eight-color mix based on a selection of brain-specific antibodies available in the laboratory and the equalization assay presented in Fig. 2. A flow diagram can be found in Extended Data Fig. 1.

Procedure

Eight-color mix design ● Timing 30 min

1 Determine targets of interest and antibodies/dyes to label those, which are available at the time of the experiment (see Table 1 for our list of validated antibodies).

Nuclei	DAPI
Cytoskeleton	Phalloidin AF488, Phalloidin AF555 and Phalloidin AF647
Microglia	IBA1 (goat IgG)
Neurons	TUBB3 (Mouse IgG2a)
Mature neurons	MAP2 (chicken IgY)
Oligodendrocytes	OLIG2 (rabbit IgG) and OLIG2-AF555 (rabbit IgG)
Astrocytes	GFAP (mouse IgG1) and GFAP (chicken IgY)
Proliferation	KI67 (rat IgG2a) and KI67-eF660 (rat IgG2a)

2 First, allocate dyes and conjugated antibodies without alternative.

405 nm		DAPI
488 nm		
514 nm		
555 nm		
568 nm		
594 nm		
633 nm		
647 nm		

3 Because we plan to use isotype-specific secondary antibodies targeting mouse isotypes, an α-mouse AF514-conjugated secondary antibody was not considered. Therefore, we filled the AF514 slot with a primary antibody raised in rabbit.

405 nm		DAPI
488 nm		
514 nm	OLIG2 (rabbit IgG)	Anti-rabbit AF514
555 nm		
568 nm		
594 nm		
633 nm		
647 nm		

4 In our case, we have only one antibody for MAP2 (chicken); therefore, GFAP (mouse) was selected to avoid using the same species twice.

5 We have AF488- and AF647-conjugated α-chicken secondary antibodies available. Taking into account the low relative intensity of AF514 (Fig. 2b), pairing it with a high-intensity primary antibody in the 488-nm slot, such as MAP2 (Fig. 2a), is not recommended. Therefore, we allocated MAP2 to the 647-nm slot.

405 nm		DAPI
488 nm		
514 nm	OLIG2 (rabbit IgG)	Anti-rabbit AF514
555 nm		
568 nm		
594 nm		
633 nm		
647 nm	MAP2 (chicken IgY)	Anti-chicken AF647

6 The unconjugated KI67 (rat) was selected because eFluor660 has a similar emission spectrum as AF647, and this slot has already been filled.

Box 2 | Eight-color-mix design walkthrough example (continued)

7 To alternate membranal and nuclear markers when possible, we used Phalloidin 488.

405 nm		DAPI
488 nm		Phalloidin 488
514 nm	OLIG2 (rabbit IgG)	Anti-rabbit AF514
555 nm		
568 nm		
594 nm		
633 nm		
647 nm	MAP2 (chicken IgY)	Anti-chicken AF647

8 From our intensity-equalization experiment (Fig. 2a), we know that GFAP (mouse IgG1), KI67 (unconjugated) and TUBB3 (mouse IgG2a) are all high-intensity primary antibodies. Therefore, we placed them together in slots 555, 568 and 594 nm excited by the same laser line 561. (Fig. 2a shows a relatively low intensity for the KI67 (rat IgG2a) antibody in adult mouse brain. Yet, the intensity of KI67 is often higher in brain tumor tissue (Fig. 6b).)

9 It is recommended that the concentration of these antibodies be optimized in relation to the intensity of the paired secondary antibody. In our case, we used a lower concentration of TUBB3 with AF555.

405 nm		DAPI
488 nm		Phalloidin 488
514 nm	OLIG2 (rabbit IgG)	Anti-rabbit AF514
555 nm	TUBB3 (mouse IgG2a)	Anti-mouse IgG2a AF555
568 nm	KI67 (rat IgG2a)	Anti-rat AF568
594 nm	GFAP (mouse IgG1)	Anti-mouse IgG1 AF594
633 nm		
647 nm	MAP2 (chicken IgY)	Anti-chicken AF647

10 Lastly, IBA1 (goat) was allocated to slot 633 nm. Several of our secondary antibodies are raised in goat. Therefore, the staining procedure is split in three sequential rounds to avoid undesired binding of α-goat-AF633 to the other secondary antibodies.

405 nm			DAPI
488 nm			Phalloidin 488
514 nm	OLIG2 (rabbit IgG)		Anti-rabbit AF514
555 nm	TUBB3 (mouse IgG2a)		Anti-mouse IgG2a AF555
568 nm	KI67 (rat IgG2a)		Anti-rat AF568
594 nm	GFAP (mouse IgG1)		Anti-mouse IgG1 AF594
633 nm	IBA1 (goat IgG)	Anti-goat AF633	
647 nm	MAP2 (chicken IgY)		Anti-chicken AF647

STAPL-3D shading correction does not require pre-acquired shading references. Instead, it estimates the shading profiles for each channel on the basis of all the tiles of the dataset. Furthermore, we detail a 3D inhomogeneity correction to account for signal artefacts from light scattering and uneven labeling in depth that often afflict 3D datasets (Procedure 2, Steps 20–25). Tiled datasets are also stitched before 3D tissue rendering (Procedure 2, Step 26).

We also provide details on mouse brain tissue preparation (Box 1), as well as recommendations for various other specimens like human tissue samples and smaller matrix-embedded organoids (Box 1). Moreover, we describe an optimized workflow for the preparation of formalin-fixed paraffin-embedded (FFPE) samples for mLSR-3D imaging, including steps for tissue deparaffinization, rehydration and antigen retrieval (Box 3).

Comparison with other methods

To also show compatibility of our mLSR-3D imaging protocol with other commonly used clearing reagents, we compared the performance of FUnGI for multi-marker imaging to aqueous-based Ce3D (clearing-enhanced 3D)[21] and CUBIC (clear, unobstructed brain imaging cocktails and

Table 1 | Antibodies and dyes compatible with mLSR-3D

Antibody/dye	Isotype, host	Sample	Dilution	Vendor, cat. no., RRID
Directly conjugated antibodies and dyes				
Anti-beta Catenin-AF568	IgG, recombinant	PK	1:100	Abcam, cat. no. ab201823
DAPI	N/A	KW/BX/BO/PK	1:750	Thermo Fisher Scientific, cat. no D3571, RRID: AB_2307445
		DX/CO/BT/EQ	1:2,000	
Anti-HER2-HiLyte Fluor 488	VHH, llama	BX	1:100	QVQ, cat. no. Q17c-lab, RRID: AB_2895305
Anti-KI67-AF488	IgG2a, rat	KW	1:100	Thermo Fisher Scientific, cat. no. 53-5698-82, RRID: AB_2802330
Anti-KI67-eFluor660	IgG2a, rat	KW/EQ	1:100	Thermo Fisher Scientific, cat. no. 50-5698-82, RRID: AB_2574235
FluoTag-X2 anti-mNeonGreen-Atto647N	sdAB, camelid	EQ	1:500	NanoTag Biotechnologies, cat. no. N3202-At647N, RRID: AB_2895306
Anti-OLIG2-AF555	IgG, rabbit	DX/EQ	1:100	Millipore, cat. no. AB9610-AF555, RRID: AB_2895307
Phalloidin-AF488	N/A	BT EQ	1:400 1:200	Thermo Fisher Scientific, cat. no. A12379
Phalloidin-Atto532	N/A	CO	1:500	Sigma-Aldrich, cat. no. 49429-10NMOL
Phalloidin-AF555	N/A	KW BX/EQ	1:500 1:200	Thermo Fisher Scientific, cat. no. A-34055
Phalloidin-AF647	N/A	KW EQ	1:1,500 1:200	Thermo Fisher Scientific, cat. no. A-22287
Anti-NCAM1-HiLyte Fluor 555	VHH, llama	KW PK	1:100 1:500	QVQ, cat. no. Q55c-lab, RRID: AB_2895308
Primary antibodies				
Anti-beta Catenin	IgG, rabbit	BO	1:200	BD Biosciences, cat. no. 610182, RRID: AB_397581
Anti-CDH1	IgG2a, rat	KW	1:250	Thermo Fisher Scientific, cat. no. 13-1900, RRID: AB_2533005
Anti-CDH1	IgG2a, mouse	KW	1:500	BD Biosciences, cat. no. 610182, RRID: AB_397581
		BX/PK/BO	1:200	
Anti-CDH6	IgG, sheep	KW/PK	1:200	R and D Systems, cat. no. AF2715, RRID: AB_883857
Anti-mouse CD31	IgG2a, rat	EQ	1:250	BD Biosciences, cat. no. 553370, RRID: AB_394816
Anti-mouse CD34	IgG2a, rat	EQ	1:250	BD Biosciences, cat. no. 553731, RRID: AB_395015
Anti-CD146	IgG, rabbit	EQ	1:250	Abcam, cat. no. ab75769, RRID: AB_2143375
Anti-EZH2	IgG, rabbit	EQ	1:100	Cell Signaling Technology, cat. no. 5246, RRID: AB_10694683
Anti-H3K27M	IgG, rabbit	EQ	1:250	Thermo Fisher Scientific, cat. no. MA5-27916, RRID: AB_2744969
Anti-Iba1	IgG, goat	BT EQ	1:200 1:250	Novus, cat. no. NB 100-1028, RRID: AB_521594
Anti-K5	IgY, chicken	BX	1:200	BioLegend, cat. no. 905903, RRID: AB_2721742
Anti K8+K18	IgG1, mouse	BX BO	1:1,000 1:200	Abcam, cat. no. ab17139, RRID: AB_443679
Anti-KI67	IgG2a, rat	KW/BX/BT	1:1,000	Thermo Fisher Scientific, cat. no. 14-5698-82, RRID: AB_10854564
		CO	1:200	
		BO/EQ	1:500	
		PK	1:1,500	
Anti-GFAP	IgY, chicken	EQ	1:1,000	Abcam, cat. no. ab4674, RRID: AB_304558
Anti-GFAP	IgG1, mouse	DX BT/EQ	1:600 1:1,000	Cell Signaling Technology, cat. no. 3670, RRID: AB_561049
Anti-MAP2	IgY, chicken	DX/BT EQ	1:200 1:250	BioLegend, cat. no. 822501, RRID: AB_2564858
Anti-N-Cadherin	IgG, sheep	EQ	1:500	R and D Systems, cat. no. AF6426, RRID: AB_10718850
Anti-NEUN	IgG, rabbit	EQ	1:1,000	Abcam, cat. no. ab104225, RRID: AB_10711153
Anti-OLIG2	IgG, rabbit	BT EQ	1:100 1:250	Millipore, cat. no. AB9610, RRID: AB_570666
Anti-PAX8	IgG1, mouse	KW/PK	1:200	GeneTex, cat. no. GTX31119, RRID: AB_2895309
Anti-PTPRZ	IgG, rabbit	EQ	1:200	Thermo Fisher Scientific, cat. no. PA5-101832, RRID: AB_2851264
Anti-RFP	IgG, rabbit	CO EQ	1:200 1:800	Rockland, cat. no. 600-401-379, RRID: AB_2209751
Anti-SIX2	IgG, rabbit	KW/PK	1:500	Proteintech, cat. no. 11562-1-AP, RRID: AB_2189084

Table continued

Table 1 (continued)

Antibody/dye	Isotype, host	Sample	Dilution	Vendor, cat. no., RRID
Anti-tubulin beta III	IgG2a, mouse	CO BT EQ	1:1,250 1:1,500 1:3,000	R and D Systems, cat. no. MAB1195, RRID: AB_357520
Anti-alpha SMA	IgG2a, mouse	BT EQ	1:1,000 1:2,000	Abcam, cat. no. ab7817, RRID: AB_262054
Anti-Vimentin	IgG2a, mouse	EQ	1:250	Millipore, cat. no. CBL202, RRID: AB_11214461
Secondary antibodies				
Anti-chicken AF488	IgG, goat	N/A	1:250	Thermo Fisher Scientific, cat. no. A-11039, RRID: AB_2534096
Anti-mouse AF488	IgG2a, goat	N/A	1:250	Thermo Fisher Scientific, cat. no. A-21131, RRID: AB_2535771
Anti-mouse AF488	IgG, donkey	N/A	1:250	Thermo Fisher Scientific, cat. no. A-21202, RRID: AB_141607
Anti-rat AF488	IgG, donkey	N/A	1:250	Thermo Fisher Scientific, cat. no. A-21208, RRID: AB_2535794
Anti-goat AF488	IgG, donkey	N/A	1:250	Thermo Fisher Scientific, cat. no. A-11055, RRID: AB_2534102
Anti-sheep AF488	IgG, donkey	N/A	1:250	Thermo Fisher Scientific, cat. no. A-11015, RRID: AB_2534082
Anti-rabbit AF488	IgG, donkey	N/A	1:250	Thermo Fisher Scientific, cat. no. A-21206, RRID: AB_2535792
Anti-mouse AF514	IgG, goat	N/A	1:250	Thermo Fisher Scientific, cat. no. A-31555, RRID: AB_2536171
Anti-rabbit AF514	IgG, goat	N/A	1:250	Thermo Fisher Scientific, cat. no. A-31558, RRID: AB_2536173
Anti-mouse CF514	IgG, donkey	N/A	1:250	Biotium, cat. no. 20483, RRID: AB_2715531
Anti-rat ATTO532	IgG, goat	N/A	1:250	Rockland, cat. no. 612-153-120, RRID: AB_10892837
Anti-mouse AF555	IgG2a, goat	N/A	1:250	Thermo Fisher Scientific, cat. no. A-21137, RRID: AB_2535776
Anti-mouse AF555	IgG, donkey	N/A	1:250	Thermo Fisher Scientific, cat. no. A-31570, RRID: AB_2536180
Anti-rat AF555	IgG, goat	N/A	1:250	Thermo Fisher Scientific, cat. no. A-21434, RRID: AB_2535855
Anti-rat AF555	IgG, donkey	N/A	1:250	Abcam, cat. no. ab150154, RRID: AB_2813834
Anti-goat AF555	IgG, donkey	N/A	1:250	Thermo Fisher Scientific, cat. no. A-21432, RRID: AB_2535853
Anti-sheep AF555	IgG, donkey	N/A	1:250	Thermo Fisher Scientific, cat. no. A-21436, RRID: AB_2535857
Anti-rabbit AF555	IgG, donkey	N/A	1:250	Thermo Fisher Scientific, cat. no. A-31572, RRID: AB_162543
Anti-mouse AF568	IgG, donkey	N/A	1:250	Thermo Fisher Scientific, cat. no. A10037, RRID: AB_2534013
Anti-mouse IgG1 AF568	IgG, goat	N/A	1:250	Thermo Fisher Scientific, cat. no. A-21124, RRID: AB_2535766
Anti-mouse IgG2a AF568	IgG, goat	N/A	1:250	Thermo Fisher Scientific, cat. no. A-21134, RRID: AB_2535773
Anti-rabbit AF568	IgG, donkey	N/A	1:250	Thermo Fisher Scientific, cat. no. A10042, RRID: AB_2534017
Anti-rat CF568	IgG, donkey	N/A	1:250	Biotium, cat. no. 20092-1, RRID: AB_10855000
Anti-rat AF568	IgG, goat	N/A	1:250	Thermo Fisher Scientific, cat. no. A-11077, RRID: AB_2534121
Anti-mouse AF594	IgG, goat	N/A	1:250	Thermo Fisher Scientific, cat. no. R37121, RRID: AB_2556549
Anti-mouse AF594	IgG, donkey	N/A	1:250	Thermo Fisher Scientific, cat. no. A-21203, RRID: AB_141633
Anti-mouse IgG1 AF594	IgG, goat	N/A	1:250	Thermo Fisher Scientific, cat. no. A-21125, RRID: AB_2535767
Anti-mouse IgG2a AF594	IgG, goat	N/A	1:250	Thermo Fisher Scientific, cat. no. A-21135, RRID: AB_2535774
Anti-rat AF594	IgG, donkey	N/A	1:250	Thermo Fisher Scientific, cat. no. A-21209, RRID: AB_2535795
Anti-goat AF594	IgG, donkey	N/A	1:250	Thermo Fisher Scientific, cat. no. A-11058, RRID: AB_2534105
Anti-rabbit AF Plus 594	IgG, donkey	N/A	1:250	Thermo Fisher Scientific, cat. no. A32754, RRID: AB_2762827
Anti-mouse AF647	IgG, donkey	N/A	1:250	Thermo Fisher Scientific, cat. no. A-31571, RRID: AB_162542
Anti-mouse AF647	IgG, rabbit	N/A	1:250	Thermo Fisher Scientific, cat. no. A-21239, RRID: AB_2535808
Anti-rat AF647	IgG, goat	N/A	1:250	Thermo Fisher Scientific, cat. no. A-21247, RRID: AB_141778
Anti-goat AF647	IgG, donkey	N/A	1:250	Thermo Fisher Scientific, cat. no. A-21447, RRID: AB_2535864
Anti-rabbit AF647	IgG, donkey	N/A	1:250	Thermo Fisher Scientific, cat. no. A-31573, RRID: AB_2536183
Anti-mouse AF660	IgG, goat	N/A	1:250	Thermo Fisher Scientific, cat. no. A-21055, RRID: AB_2535722
Anti-mouse AF633	IgG, goat	N/A	1:250	Thermo Fisher Scientific, cat. no. A-21052, RRID: AB_2535719
Anti-rat AF633	IgG, goat	N/A	1:250	Thermo Fisher Scientific, cat. no. A-21094, RRID: AB_2535749
Anti-goat AF633	IgG, donkey	N/A	1:250	Thermo Fisher Scientific, cat. no. A-21082, RRID: AB_2535739
Anti-sheep AF633	IgG, donkey	N/A	1:250	Thermo Fisher Scientific, cat. no. A-21100, RRID: AB_2535754
Anti-chicken AF647	IgG, goat	N/A	1:250	Thermo Fisher Scientific, cat. no. A-21449, RRID: AB_2535866
Anti-mouse AF700	IgG, goat	N/A	1:250	Thermo Fisher Scientific, cat. no. A-21036, RRID: AB_2535707

Details on the tissue type in which antibodies or dyes have been used are listed in the sample column. Listed secondary antibodies work with all tissue. BO, breast cancer organoids; BT, brain tumors; BX, breast cancer xenografts; CO, cerebral organoid; DX, diffuse midline glioma xenograft; EQ, equalization assay; KW, human fetal kidney and Wilms tumor; N/A, not applicable; PK, paraffin-embedded human fetal kidney.

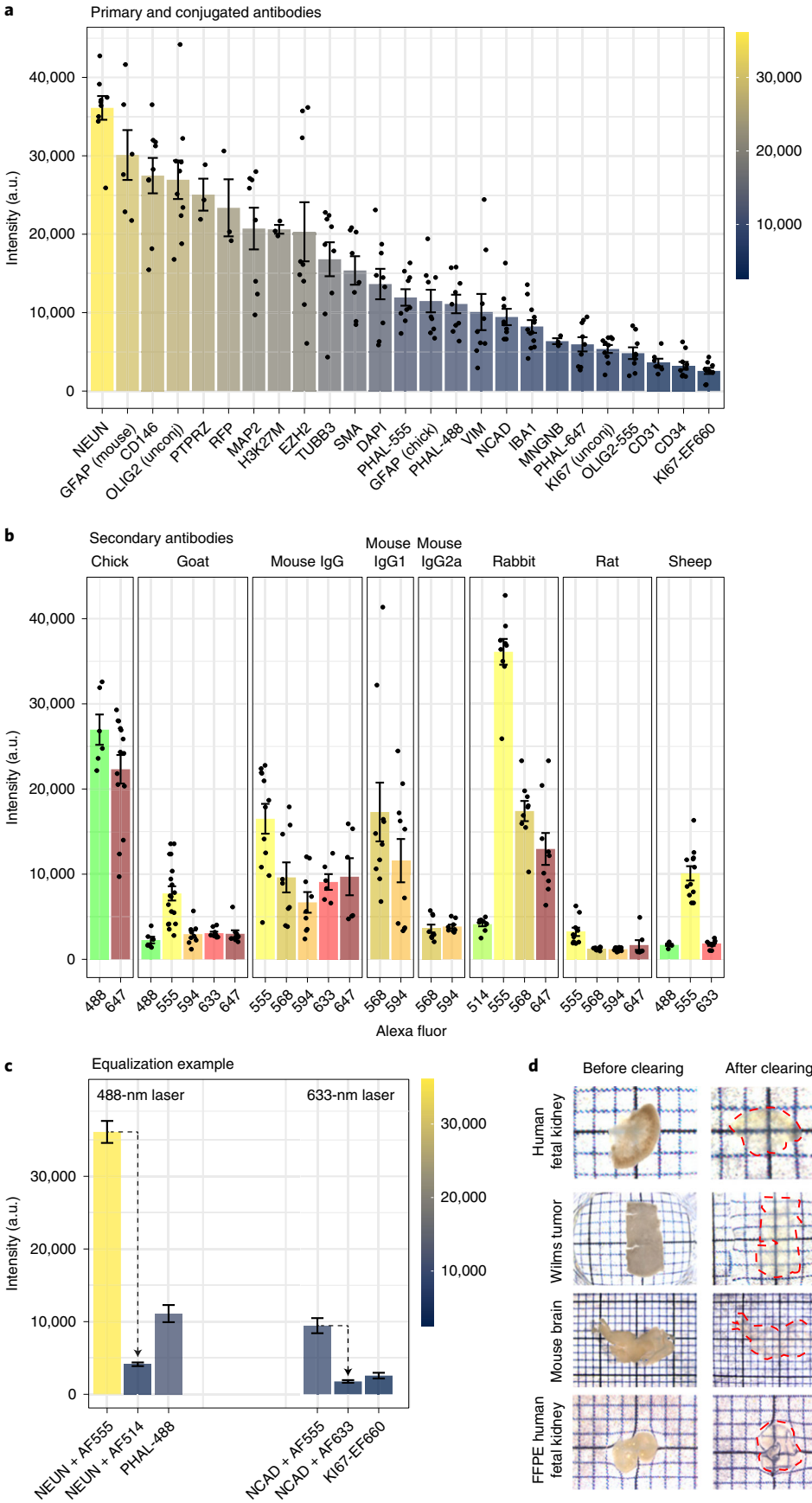
a
Primary and conjugated antibodies
Intensity (a.u.)
40,000
30,000
20,000
10,000
0
NEUN
GFAP (mouse)
CD146
OLIG2 (unconj)
PTPRZ
RFP
MAP2
H3K27M
EZH2
TUBB3
SMA
DAPI
PHAL-555
GFAP (chick)
PHAL-488
VIM
NCAD
IBA1
MNGNB
PHAL-647
KI67 (unconj)
OLIG2-555
CD31
CD34
KI67-EF660
b
Secondary antibodies
Chick
Goat
Mouse IgG
Mouse IgG1
Mouse IgG2a
Rabbit
Rat
Sheep
Alexa fluor
c
Equalization example
488-nm laser
633-nm laser
NEUN + AF555
NEUN + AF514
PHAL-488
NCAD + AF555
NCAD + AF633
KI67-EF660
d
Before clearing
After clearing
Human fetal kidney
Wilms tumor
Mouse brain
FFPE human fetal kidney

◀ **Fig. 2 | mLSR-3D equalization assay and FUnGI clearing. a**, Fluorescent intensities of primary antibodies tested on brain tissue. Accumulative data from $n = 1$–4 independent experiments with one to three areas per sample imaged for each antibody. Data are presented as mean values +/− s.e.m. Bar colors represent intensities. Mouse, rabbit, goat, rat and sheep unconjugated primary antibodies were imaged with AF555 secondary antibody. Chicken primary antibodies were imaged with AF647 secondary antibody. Antibody species are displayed in Table 1. **b**, Fluorescent intensity obtained for secondary antibodies. Accumulative data from $n = 1$–3 independent experiments with one to three areas per sample imaged for each antibody. Data are presented as mean values +/− s.e.m. Bar colors represent different fluorophores. The primary antibodies used were chicken-MAP2, goat-IBA1, mouse IgG-TUBB3, mouse IgG1-GFAP, mouse IgG2a-TUBB3, rabbit-NEUN, rat-CD34 and sheep-NCAD. **c**, Equalization of NEUN to Phalloidin-AF488, both excited by the 488-nm laser (left) and NCAD to KI67-eFluor660, both excited by the 633-nm laser (right). Accumulative data from $n = 1$–3 independent experiments with three areas per stained sample imaged for each antibody. Data are presented as mean values +/− s.e.m. Colors represent intensity. Dotted arrows represent intensity equalization. **d**, Widefield microscopic images of various tissues before and after optical clearing by FUnGI. Squares represent 1 mm.

Box 3 | FFPE tissue preparation for mLSR-3D

This box describes FFPE sample-specific preprocessing steps required for successful integration with the standard mLSR-3D protocol.

Procedure

FFPE tissue preparation ● Timing 18 h

1 Pre-heat 30 ml of xylene to 37 °C in a 50-ml Falcon tube by using a water bath.
! CAUTION Xylene is harmful if inhaled or if it comes in contact with skin, and it causes serious eyes damage. Handle in a fume hood with protective gloves and wear eye goggles and a laboratory coat.

2 Deparaffinize the tissue block by submerging it in the Falcon tube containing pre-heated xylene. Incubate the tube for 1 h at 37 °C in a water bath.
▲ CRITICAL STEP The tissue block will detach from the back of the histology cassette during this incubation step. To simplify handling, we recommend transferring the tissue in the histology cassette and closing the lid of the cassette.

3 Transfer the tissue to a new 50-ml Falcon tube containing 30 ml of room temperature xylene and incubate on a roller bank at room temperature for 1 h.

4 Gradually rehydrate tissue in successive ethanol solutions ranging from 100%, 90%, 80% to 70% (vol/vol) ethanol diluted in distilled water (final volume of 30 ml). Incubate each step for 1 h at room temperature on a roller bank. Use a new Falcon tube for each ethanol dilution and transfer the tissue from one tube to another.

5 Transfer the deparaffinized and rehydrated tissue to a Falcon tube containing 30 ml of PBS and incubate at 4 °C overnight on a roller bank.

Antigen retrieval ● Timing 3 h

▲ CRITICAL Heat-induced epitope retrieval is a crucial step, because without it many antibodies do not work, whereas further immunostaining, clearing and imaging steps are equal to the general mLSR-3D protocol (Fig. 5a).

▲ CRITICAL For tissue larger than 500 µm, we recommend sectioning the sample by using a vibrating blade microtome as described in step 4 of the tissue preparation section (Box 1).

6 Preheat 100 ml of 1× Dako target retrieval solution pH 9 to 65 °C in a glass beaker by using a heating plate.

7 Transfer intact tissue into the beaker and raise the temperature to 95 °C. Monitor temperature with a thermometer and cover the beaker with aluminum foil.
▲ CRITICAL STEP If a tissue section is used, transfer the sample into a histology cassette chamber to avoid any damage during handling. Keep the section in this container for steps 8 and 9.

8 Wait for the temperature to reach 95 °C and then incubate the sample for 20 min.

9 Remove the beaker from the heat source and let the solution and sample cool down for 20 min at room temperature.

10 Wash the tissue by transferring it to a 15-ml Falcon tube containing 10 ml of PBT by using forceps or a flat spoon and incubate for 15 min at room temperature on a roller bank.

11 Repeat washing step 10 once.

If the tissue is of significant size (500 µm and larger) and requires further slicing, proceed from step 4 in Box 1. For smaller samples, proceed with the equalization assay (Procedure 1, Step 1) or the main mLSR3D protocol (Procedure 2, Step 1).

computational analysis)[33] and solvent-based iDISCO (immunolabeling-enabled three-dimensional imaging of solvent-cleared organs)[17] (Extended Data Fig. 2 and Supplementary Methods). Although this revealed similar results between FUnGI and Ce3D, iDISCO performed less well regarding brightness and quality of some membranal markers, in addition to shrinking the tissue. Furthermore, iDISCO was not compatible with F-actin, our main marker used for visualizing tissue architecture. With our protocol and in our hands, CUBIC performed worse, showing specific signal only for DAPI, as well as dim fluorescence for nuclear marker SIX2. In addition, the tissue and, specifically, nuclei seemed deformed, generally appearing enlarged. This demonstrates that, although FUnGI is less potent in absolute clearing potential than iDISCO or CUBIC, it remains the clearing method of choice for spectral 3D imaging at high resolution using confocal microscopy, because obtained tissue architecture preservation and antibody compatibility is essential for downstream single-cell profiling, a main application of our protocol showcased in Fig. 1.

3D microscopy approaches are generally affected by a trade-off in resolution versus volume. Objective lenses with long working distance usually have lower resolving capabilities. In addition, increasing resolution results in longer imaging time and larger data size. This is especially problematic

Fig. 3 | mLSR-3D imaging of fetal kidney, Wilms tumor, breast cancer xenograft and organoids. a, 3D rendering of human fetal kidney (12 weeks of gestation) labeled for DAPI (white), KI67 (magenta), PAX8 (yellow), NCAM1 (blue), SIX2 (green), CDH1 (gray), CDH6 (orange) and F-ACTIN (signal intensitiy gradient: red-yellow-white). **b**, Wilms tumor labeled for DAPI (not shown), KI67 (green), PAX8 (gradient: red-yellow-white), NCAM1 (blue), SIX2 (magenta), CDH1 (gray), CDH6 (orange) and F-ACTIN (cyan). **c**, Breast cancer xenograft labeled for DAPI (gray), KI67 (cyan), CDH1 (yellow), K8/18 (blue), K5 (red), HER2 (orange) and F-ACTIN (green). **d**, Breast cancer organoids labeled for DAPI (gray), KI67 (green), B-CAT (yellow), CDH1 (red) and K8/18 (blue). Scale bars, 500 µm. Overview image (left) and magnification of indicated area (white square) (right). Panels **a** and **b** adapted from ref. [26], Springer Nature Limited. ▶

in 3D, because a doubling of the resolution in three dimensions leads to an (2 × 2 × 2) eight-fold increase in scan time and volumetric data size[34]. Similarly, increasing the number of imaged channels by repetitive illumination scans drastically increases *z*-stack scan time (Supplementary Table 1). As compared to previous high-dimensional imaging methods that rely on multiple acquisition scans and post-acquisition compensation[31,35], mLSR-3D allows for better image quality by drastically reducing acquisition time, photo-bleaching induced by repetitive illumination and file size. Together, this expedites volumetric high-dimensional imaging, as demonstrated in Supplementary Table 1 and Extended Data Fig. 3.

Applications of the method

Large-scale single-cell resolution 3D imaging was originally developed to reveal intraclonal plasticity in mammary tumors[7]. Additional studies later demonstrated versatility of the protocol by using it to unveil processes of intestinal enteroendocrine differentiation[36], as well as volumetric imaging of organoid models[37–41]. More recently we enhanced this volumetric imaging technology by exploiting multispectral imaging and designing a complete analysis toolbox, STAPL-3D, enabling precise mapping of cellular heterogeneity in Wilms tumor[26] and its healthy tissue counterpart. Here, we additionally show applicability of our method for phenotyping various healthy and tumor tissues (Figs. 3 and 4).

Limitations

With mLSR-3D being a confocal imaging method, it is limited by the constraints of this microscope modality. Scan time depends on desired resolution, as well as tissue size, and can therefore be a hurdle for larger specimens. Imaging depth is limited by the working distance of the objectives (Supplementary Table 2). Therefore, for samples larger than the working distance, mLSR-3D needs to be performed on thick sections. Volumetric organ reconstruction after tissue sectioning is possible through post-processing alignment of consecutive tick slice datasets[42]. However, the end result is prone to deformations, as well as loss of some tissue, because of the sectioning.

In general, working distance decreases when the magnification and the numerical aperture (NA) increase. This means that obtaining sufficient resolution in *z*-dimension for the envisioned downstream application of 3D imaging data requires a balance between imaging depth and *z*-resolution. Light-sheet microscopy could potentially improve 3D imaging capacity in terms of depth, as compared with confocal microscopy, and light-sheet systems with multispectral capabilities have been reported[30,43,44]. However, large-volume light-sheet data suffer from reduced resolution, which might hamper detailed downstream quantification analyses. Because of such envisioned high-resolution data applications and restriction of ligh-sheet microscopy in this regard, mLSR-3D was specifically tailored to confocal microscopy. However, we expect the eight-color labeling, intensity equalization strategy and 3D inhomogeneity correction of mLSR-3D to be of added value to multispectral light-sheet experiments as well. Next to light-sheet technology, two-photon microscopy could similarly improve the limited depth of confocal imaging, and we demonstate that it is technically compatible with our mLSR-3D protocol (Extended Data Fig. 4). Yet, it remains challenging to equally excite multiple fluorophores with the typical two or three laser lines of two-photon systems.

Thus, despite being specifically designed for confocal imaging, experiments using other microscope modalities can directly benefit from the mLSR-3D protocol as well. Our equalization assay, immunostaining, FUnGI optical clearing and image-processing steps can be applied with minimal adaptations, depending on the specific experimental requirements. For now, the mLSR-3D protocol as described is limited to eight colors by the software of the microscope. However, future improvements in unmixing algorithms[24] can be expected to further increase this number of markers.

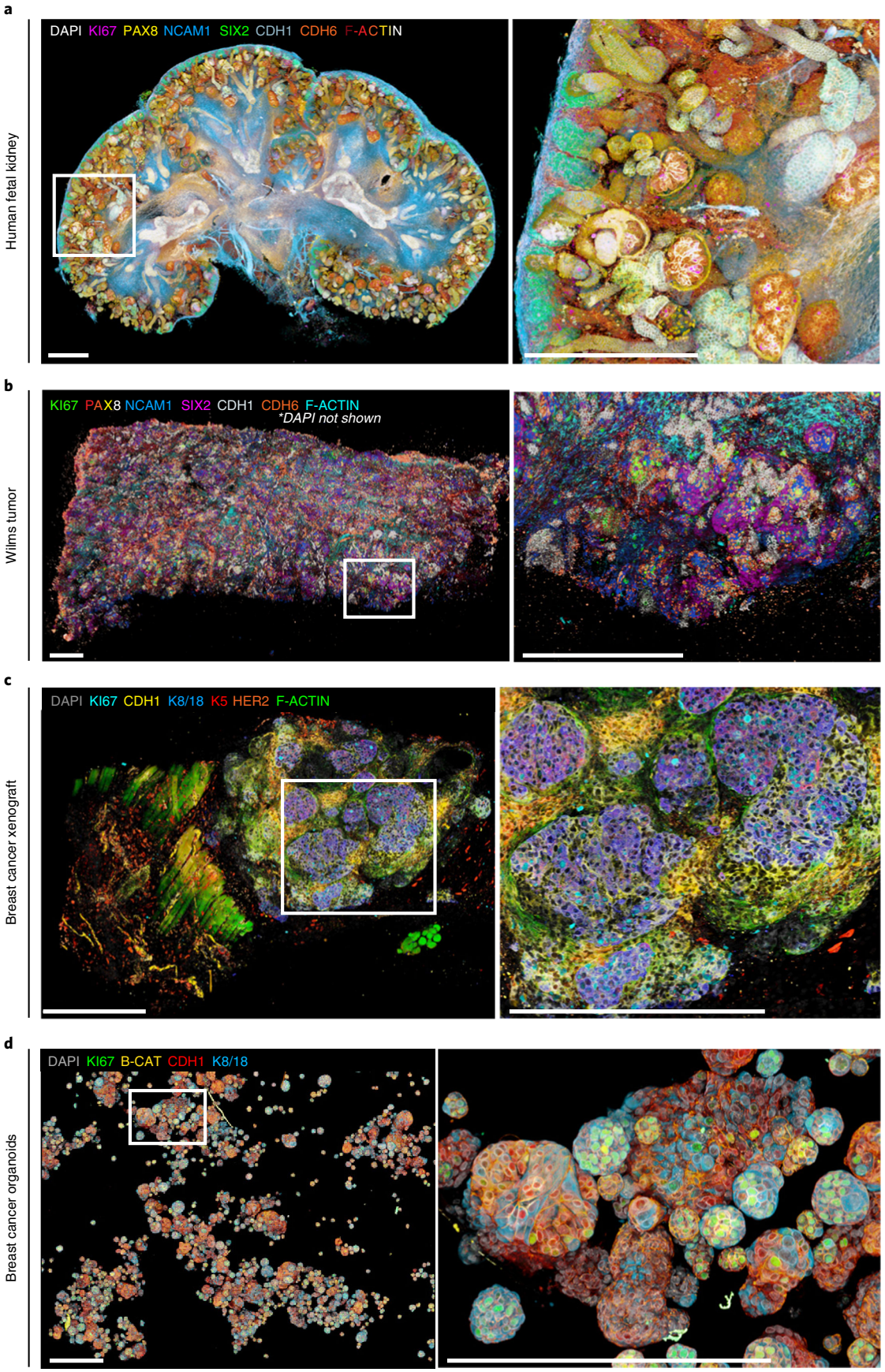
a
Human fetal kidney
DAPI KI67 PAX8 NCAM1 SIX2 CDH1 CDH6 F-ACTIN
b
Wilms tumor
KI67 PAX8 NCAM1 SIX2 CDH1 CDH6 F-ACTIN
*DAPI not shown
c
Breast cancer xenograft
DAPI KI67 CDH1 K8/18 K5 HER2 F-ACTIN
d
Breast cancer organoids
DAPI KI67 B-CAT CDH1 K8/18

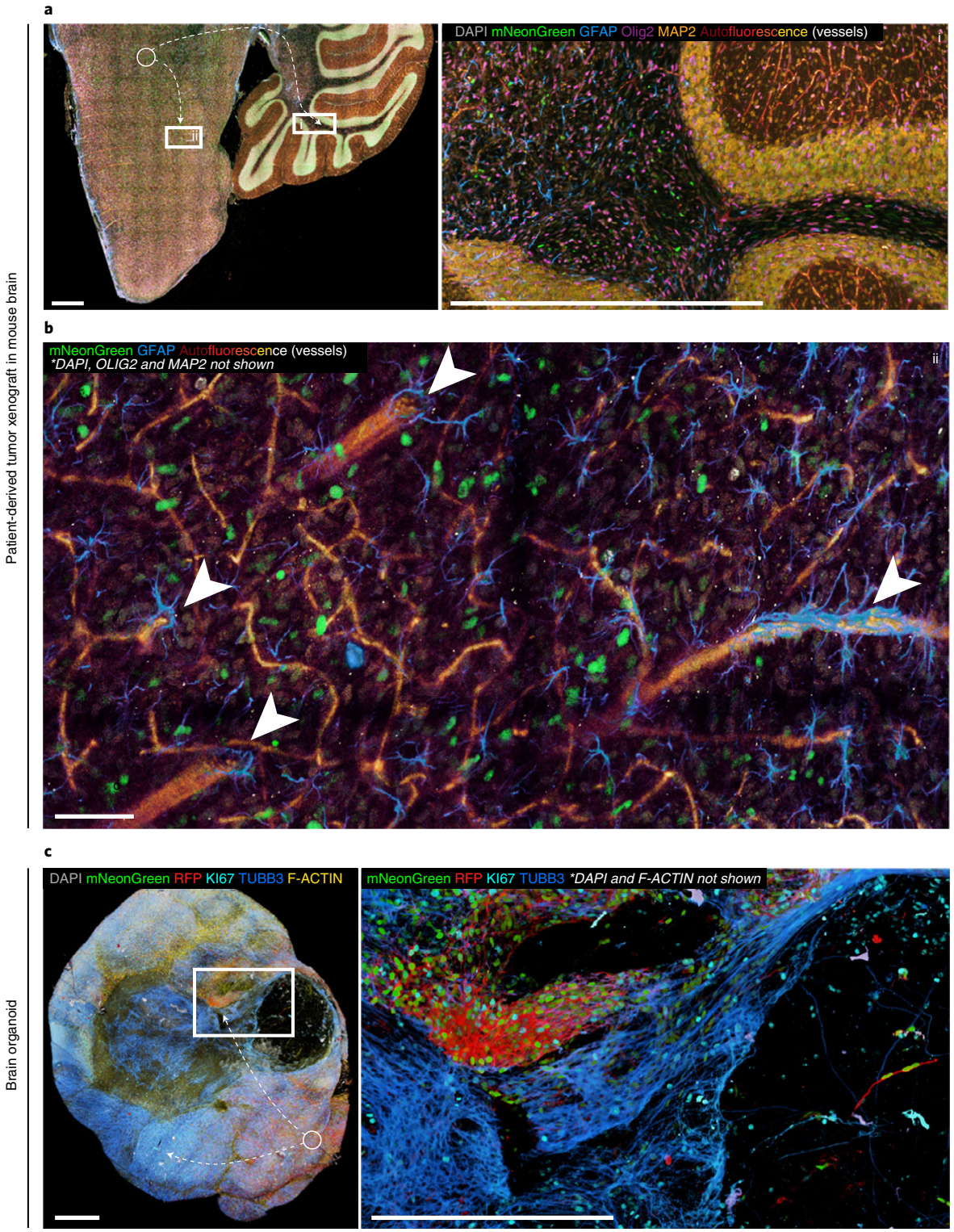

Fig. 4 | mLSR-3D imaging of brain tissue and organoids. a, 3D rendering of a mouse brainstem and cerebellum with a patient-derived diffuse midline glioma (DMG) xenograft in the pontine region; DAPI (gray), mNeonGreen-positive DMG tumor cells (green), GFAP (blue), Olig2 (purple), MAP2 (orange) and autofluorescence of blood vessels (signal intensity gradient: red-yellow-white). Scale bars, 500 µm. Overview image (left) and magnification of indicated area i (white square) (right). The white circle indicates the injection site of DMG tumor cells, and arrows indicate mNeonGreen-positive DMG tumor cells distant from the injection site. **b**, White arrowheads indicate GFAP-positive astrocytes at the gliovascular interface of magnified area ii in panel **a** (white square). Scale bar, 50 µm. **c**, 3D representation of a cerebral organoid fused with a patient-derived DMG organoid; DAPI (gray), mNeonGreen-positive tumor cell nuclei (green), RFP-positive membrane (red), KI67 (cyan), Tubulin beta 3 (TUBB3) (blue) and F-actin (yellow). Scale bars, 500 µm. Overview image (left) and magnification of indicated area (white square) (right). The white circle indicates the fusion site, and dashed arrows point toward mNeonGreen-positive tumor cells distant from the fusion site.

Expertise, microscope and data infrastructure needed to implement the protocol

Spectral imaging with unmixing during acquisition requires a specialized confocal microscope with spectral detector and software that allows 'on-the-fly' processing of images that are being acquired. Therefore, the protocol is designed for confocal microscopes equipped with a spectral detector and real-time unmixing capabilities, available on Zeiss (e.g., LSM780, LSM880 and LSM980) and Nikon (e.g., A1-DUS) microscopes. In addition, because the resulting high-dimensional datasets can be up to a terabyte in size, implementation of the protocol requires powerful workstations and high-performance computing clusters for image processing and analysis (see Materials). In terms of user expertise, a basic understanding of Python programming language is required to run the equalization assay analyses and imaging preprocessing pipeline. In addition, handling and visualizing large high-dimensional datasets and mining the large amount of information obtained requires acquaintance with the Imaris (Bitplane Oxford-Instrument) image analysis software for 3D visualization and data processing.

Materials

Biological Materials

- Fresh and FFPE-embedded human fetal kidney **! CAUTION** Any experiments using human material must conform to relevant institutional and national regulations, and informed consent must be obtained. Human fetal kidney was obtained from women undergoing elective abortion and donated through written informed consent, with approval from the Medical Ethics Committee from the Leiden University Medical Center (P08.087).
- Human breast cancer organoids: obtained from the Hubrecht Organoid Technology (www.hub4organoids.nl) biobank **! CAUTION** Compliance with the Dutch Medical Research Involving Human Subjects Act was ensured for every material obtained by requesting the necessary authorizations by the ethical committee of the UMC Utrecht. When appropriate, informed consent was obtained from donors.
- Human Wilms tumor and pediatric gliomas: obtained from the biobank of the Princess Máxima Center (PMCLAB2019.037) **! CAUTION** Material was obtained with the necessary authorizations by the ethical committee of the UMC Utrecht and in compliance with the Dutch Medical Research Involving Human Subjects Act.
- Breast cancer and diffuse midline glioma (DMG) tissue: obtained from xenograft mouse models **! CAUTION** Any experiments involving live mice must conform to relevant institutional and national regulations. Here, work was approved by the Animal Welfare Committee of the Princess Máxima Center and established in compliance with both local and international regulations.
- Human embryonic stem cells used for the generation of cerebral organoid: H9 (hPSCReg ID: WAe009-A)[45] kindly provided by Marcel Kool **! CAUTION** Any experiments using human stem cells must comply with relevant institutional and national regulations. The cell lines used in your research should be regularly checked to ensure that they are authentic and are not infected with mycoplasma.

Reagents

- Alfa Aesar urea, ultrapure 99% (Thermo Fisher Scientific, cat. no. 15447069)
- BSA (Sigma-Aldrich, cat. no. A3059)
- D-(−)-Fructose (Sigma-Aldrich, cat. no. F0127)
- Dako target retrieval solution pH 9 (Agilent, cat. no. S237584-2)
- EDTA (Invitrogen, cat. no. 15576-028) **! CAUTION** EDTA causes serious eye irritation. Handle with rubber gloves and wear protective goggles and a laboratory coat.
- Ethanol, 100% (BOOM, cat. no. 84028185.2500)
- Glycerol (Sigma-Aldrich, cat. no. G5516)
- HCl, 37% (Acros Organics, cat. no. 124620010) **! CAUTION** HCl is a corrosive substance causing severe skin burns and eye damage. It is toxic if inhaled. Handle in a fume hood with protective gloves and wear eye goggles and a laboratory coat.
- Paraformaldehyde (PFA) (Sigma-Aldrich, cat. no. P6148) **! CAUTION** PFA is a toxic substance if swallowed or inhaled or if it comes in contact with skin. Handle in a fume hood with protective gloves and wear eye goggles and a laboratory coat.
- PBS (Thermo Fisher Scientific, cat. no. 10010002)
- Primary antibodies, user defined (successfully used antibodies for mLSR-3D are listed in Table 1)

- Secondary antibodies, user defined (successfully used secondary antibodies for the labeling of primary antibodies are listed in Table 1)
- Silicon sealant (Griffon, cat. no. S-200)
- SDS (Merck, cat. no. L3771) **! CAUTION** SDS is a harmful substance if swallowed. It causes skin and eye irritation. Handle in a fume hood with protective gloves and wear eye goggles and a laboratory coat.
- NaOH, 10 M (Sigma-Aldrich, cat. no. 567530) **! CAUTION** NaOH is a corrosive substance causing severe skin burns and eye damage. Handle in a fume hood with protective gloves and wear eye goggles and a laboratory coat.
- Tris (Thermo Fisher Scientific, cat. no. 11486631) **! CAUTION** Tris causes serious eye and skin irritation. Handle with protective gloves and wear goggles and a laboratory coat.
- Triton X-100 (Sigma-Aldrich, cat. no. T8787) **! CAUTION** Triton X-100 is a harmful substance if swallowed. It causes serious skin and eye irritation. Handle in a fume hood with protective gloves and wear eye goggles and a laboratory coat.
- Tween-20 (Sigma-Aldrich, cat. no. P9416)
- UltraPure low melting point agarose (Invitrogen, cat. no. 16520)
- Xylene (BOOM, cat. no.76052683.5000) **! CAUTION** Xylene is a potentially fatal substance if swallowed. It is harmful if inhaled or if it comes in contact with skin, and it causes serious eye damage. Handle in a fume hood with protective gloves and wear eye goggles and a laboratory coat.

Equipment

- 10-ml syringe (BD, cat. no. 300912)
- Bone scissors (Fine Science Tools, cat. no. 14185-09)
- Conventional needles 26 gauge × 1/2 inch (BD, cat. no. 305111)
- Disposable scalpel (Swann-Morton, cat. no. 6601)
- Dumont #5 forceps (Fine Science Tools, cat. no. 11251-20)
- Histology cassettes (VWR, cat. no. 18000)
- Moria Iris forceps (Fine Science Tools, cat. no. 11373-12)
- Peel-A-Way embedding molds (Sigma-Aldrich, cat. no. E6032)
- JB Nova water bath (Grant, cat. no. JBN5)

Transcardial perfusion and tissue dissection/sectioning

- Leica M80 stereomicroscope (Fisher Scientific, cat. no. 11960798)
- Vibrating blade microtome, Leica VT 1200S (Leica, cat. no. 14048142065)

Immunostaining

- 24-well cell culture plate (Greiner Bio-One, cat. no. 662160)
- 6-well cell culture plate (Greiner Bio-One, cat. no. 657160)
- 96-well cell culture plate (Greiner Bio-One, cat. no. 655088)
- Cellstar conical tubes, 15 ml (Greiner Bio-One, cat. no. 188271)
- Cellstar conical tubes, 50 ml (Greiner Bio-One, cat. no. 227261)
- Orbital shaker (VWR, cat. no. 444-2900)
- Positive displacement pipette, MICROMAN E M100E, 10–100 µl (Gilson, cat no. FD10004)
- Rocking platform (VWR, cat. no. 10860)
- Roller bank IKA Roller 10 (IKA, cat. no. 0004013000)
- Safe-Lock centrifuge tubes, 1.5 ml (Eppendorf, cat. no. EP0030123611)
- Safe-Lock centrifuge tubes, 2 ml (Eppendorf, cat. no. 0030120094)

Equalization assay

- FieldMate laser power meter (Coherent, cat. no. SKU 1098297)
- Glass-bottom eight-well µ-Slides (Ibidi, cat. no. 80827)
- PCR eight-tube strip (Greiner Bio-One, cat. no. 671221)

Slide preparation

- Cover slips, 24 × 60 mm #1.5 SPEZIAL (VWR, cat. no. 631-0853)

Confocal microscope and objectives

- Zeiss LSM880 (25× NA 0.8 multi-immersion; working distance of 570 µm)

Image processing

- Analysis workstation (64-bit, Intel Xeon 5222 3.8 2,666 MHz 8 cores, 1 terrabyte DDR4 RAM, NVIDIA QUADRO RTX 4000 8 GB)
- Imaris ×64 9.6.1 (Bitplane Oxford-Instrument)
- STAPL-3D (dev1.0.0) (https://github.com/RiosGroup/STAPL3D)
- Zeiss ZenBlack 2.3 sp1
- Zeiss ZenBlue 2.6 Desk

Reagent setup

EDTA (0.5 M, 100 ml)

Dissolve 18.6 g of EDTA and 2.5 g of NaOH in 80 ml of distilled water. Using 1 M NaOH, adjust pH to 8 and fill to 100 ml final volume with distilled water. Store at room temperature (21 °C) for ≤6 months.

Tris buffer (1 M, 500 ml)

Dissolve 60.55 g of Tris in 42 ml of HCL (36–38% (wt/vol)), add 300 ml of distilled water and adjust the pH to 8. Fill up to a final volume of 500 ml by adding distilled water. Store at room temperature for ≤6 months.

PFA (4% (wt/vol), 500 ml)

Dissolve 20 g of PFA in 500 ml of 60 °C PBS by using a magnetic stirrer. Cool on ice and adjust the pH to 7.4 by adding 10 M NaOH or HCl. The preparation time is 4 h. PFA 4% (wt/vol) can be stored at −20 °C for ≤2 months. **! CAUTION** PFA is a toxic substance if swallowed or inhaled or if it comes in contact with skin. Prepare under a fume hood and wear rubber gloves, protective eye goggles and a laboratory coat. **▲ CRITICAL** PFA should not be heated above 60 °C, to avoid degradation.

PBS-Tween (PBT, 0.1% (vol/vol), 1 liter)

Dissolve 1 ml of Tween-20 in 1 liter of PBS by using a magnetic stirrer. The preparation time is 10 min. PBT can be stored at 4 °C for ≤4 weeks.

Washing buffer 1 (WB1, 1 liter)

Dissolve 2 ml of Tween-20, 2 ml of 10% (vol/vol) SDS, 2 ml of Triton X-100 and 2 g of BSA in 1 liter of PBS by using a magnetic stirrer. The preparation time is 10 min. Store WB1 at 4 °C for ≤2 weeks.

Washing buffer 2 (WB2, 1 liter)

Dissolve 2 ml of 10% (vol/vol) SDS, 1 ml of Triton X-100 and 2 g of BSA in 1 liter of PBS by using a magnetic stirrer. The preparation time is 10 min. Store WB2 at 4 °C for ≤2 weeks.

Fructose-glycerol clearing (FUnGI, 220 ml)

Mix 110 ml of glycerol with 20 ml of distilled water, 2.2 ml of 1 M Tris buffer pH 8 and 440 µl of 0.5 M EDTA. Add 50 g of fructose and dissolve with a magnetic stirrer at room temperature and in the dark until a clear solution is obtained. Subsequently, add an additional 49 g of fructose and mix well until dissolved. Finally, add 33.1 g of urea and mix well until dissolved. Final concentrations are as follows: 50% (vol/vol) glycerol, 9.4% (vol/vol) dH_20, 1.1 mM EDTA, 10.6 mM Tris buffer, 2.5 M fructose and 2.5 M urea. The preparation time is 1 d. Store FUnGI at 4 °C in the dark for ≤4 weeks. **▲ CRITICAL** Do not heat up FUnGI, to avoid fructose oxidation.

Procedure

Procedure 1: equalization assay

▲ CRITICAL The following procedure includes the aquisition of spectral references required for spectral unmixing, as well as the detailed steps to perform an equalization assay. This procedure must be performed once for each type of tissue. We recommend performing the equalization assay in triplicate to insure optimal results (excluding the spectral reference aquisition (Steps 13 and 14)).

Sample dissection and blocking ● Timing 6 h

1 Cut the fixed tissue (see Box 1 for tissue preparation) into small cubes of 0.5 mm^3 with a scalpel under a stereo microscope. Using forceps, transfer each sample in a different well of a 96-well plate containing 100 µl of PBT.

▲ CRITICAL STEP Depending on the number of antibodies and dyes included in the equalization assay, a large amount of tissue might be required. 96-well plates are used to reduce antibody consumption and enable high-throughput processing using multi-channel pipettes. Different regional structures within the same tissue can have significant variations in marker expression. Consistency in the tissue areas dissected for the equalization assay is key.

■ PAUSE POINT Tissue can be stored in PBT at 4 °C for ≤2 d. However, fresh tissue performs best, and the protocol should be continued as soon as possible.

2 Block the samples by replacing PBT with 100 µl of blocking solution WB1. Incubate at 4 °C for 4 h on an orbital shaker.

High-throughput single staining ● Timing 44 h

▲ CRITICAL To increase consistency, each primary antibody should, if possible, be imaged with a secondary antibody coupled to the same fluorophore. Similarly, all secondary antibodies (fluorophores and species) should, if possible, be imaged with primary antibodies that are known to work well in the desired tissue.

3 Prepare single-stain primary antibody dilution by adding 120 µl of WB2 in a PCR strip and adding the primary antibody at the appropriate dilution (Table 1). Resuspend by pipetting up and down with a multi-channel pipette.

▲ CRITICAL STEP For conjugated primary antibodies or dyes, skip the addition of antibodies for this first immunostaining round and add only 120 µl of WB2 to the PCR strip.

4 Remove WB1 from each well and replace with 100 µl of primary antibody mix by using a multi-channel pipette. Incubate at 4 °C overnight on an orbital shaker.

5 Remove primary antibody mix and wash tissue with 200 µl of WB2 for 1 h at 4 °C on an orbital shaker. Repeat this washing step two additional times for ≥1 h.

▲ CRITICAL STEP Careful washing is important to reduce background signal from nonspecific primary antibody binding.

■ PAUSE POINT Once washed, tissue can be stored in WB2 at 4 °C for 2 d or over the weekend. However, fresh tissue performs best, and the protocol should be continued as soon as possible.

6 Prepare single-stain fluorophore mixes by adding 120 µl of WB2 in a PCR strip and add the secondary antibody, conjugated primary or fluorescent dye at the appropriate dilution (Table 1). Mix well by pipetting up and down with a multi-channel pipette.

7 Remove WB2 from each well and add 100 µl of the prepared secondary antibody, conjugated primary or fluorescent dye mix by using a multi-channel pipette. Incubate in the dark at 4 °C overnight on an orbital shaker.

8 Remove WB2 from each well and wash tissue with 200 µl of WB2 for 1 h at 4 °C on an orbital shaker. Repeat this washing step two additional times for ≥1 h.

▲ CRITICAL STEP Keep samples in the dark for all the subsequent steps. Proceed immediately with tissue clearing and imaging to avoid any loss of signal and guarantee optimal-intensity quantifications.

Tissue clearing by using a FUnGI gradient ● Timing 15 h

9 Prepare a dilution of 33% (vol/vol) FUnGI in WB2 and 66% (vol/vol) FUnGI in WB2. Bring FUnGI stock to room temperature for reduced viscosity. Dilute accordingly and homogenize on a roller bank or by vortexing briefly. Keep the required amount of 33%, 66% and 100% (vol/vol) FUnGI solution at room temperature.

▲ CRITICAL STEP Always make fresh FUnGI dilutions on the day of clearing. BSA in the dilutions should not be kept at room temperature for more than 24 h. FUnGI clearing agent is viscous and should be dispensed slowly to avoid bubble formation. Throughout the clearing process the tissue will gradually become translucent and sink to the bottom of the well.

10 To clear tissue by using a FUnGI gradient, replace WB2 with 150 µl of 33% (vol/vol) FUnGI solution by using a multi-channel pipette and incubate for 1 h at room temperature with mild rocking or shaking. Carefully remove 33% (vol/vol) FUnGI solution by using a multi-channel pipette and replace with 150 µl of 66% (vol/vol) FUnGI solution.

11 Using forceps, transfer tissue cubes in a new 96-well plate with wells containing 150 µl of 100% (vol/vol) FUnGI solution. Incubate at 4 °C overnight with mild rocking.

▲ CRITICAL STEP 66% and 100% (vol/vol) FUnGI solutions are too viscous to pipette accurately with regular pipettes. Because the exact quantity is not critical, it is possible to complete this step by using a regular or multi-channel pipette. However, we recommend using positive displacement pipettes and always ensuring that the tissue is completely covered with FUnGI solution.

12 Transfer the cleared tissue into an imaging chamber (e.g., glass-bottom eight-well μ-slide, Ibidi) and ensure that the sample is not floating on a layer of FUnGI solution by pipetting off the excess.
? TROUBLESHOOTING

Spectral signature reference library acquisition ● Timing 2 h

▲ CRITICAL Spectral imaging has been specifically optimized for the Zeiss LSM880 confocal microscope using the online-fingerprinting module. We recommend using the same objective for the acquisition of images for the reference spectra, intensity-equalization assay and the general mLSR3D experiment. Throughout this protocol, we use a 25× oil-immersion objective.

13 Aquire one spectral signature for every unique fluorophore. Using the Lambda Mode, choose a single plane containing the signal of interest and acquire individual lambda stack images. Using the same objective and acquisition parameters as in the intended experiment, except for laser power, is recommended.
Recommendations for mLSR-3D are:
- A high-NA objective with >500-μm working distance
- Voxel size of 300–400 nm in *x,y* and 1,000–1,400 nm in *z*
- 1–2-μs pixel dwell time
- 16-bit images

14 Under the Unmixing tab, use the Auto find (1 dye) to obtain the spectral reference signature for each separate fluorophore. Save the spectral signatures in the Spectra Database for subsequent use in the Online Fingerprinting Mode.
? TROUBLESHOOTING

Imaging for intensity-equalization assay ● Timing 4–5 h

▲ CRITICAL The output power of some microscope lasers can fluctuate or decline over the microscope's lifetime. To ensure optimal reproducibility between equalization-assay replicates, the laser powers are measured by using a laser power meter at the beginning of the assay, and the imaging laser intensity is corrected for the shift in power output over time. This also allows for the addition of further intensity measurement data from a new antibody at a later time point, without having to repeat the entire experiment.

15 Activate the Online Fingerprinting Mode, select the saved spectral reference for each one of the fluorophores that are part of the equalization assay and activate the corresponding lasers.

16 Determine the set of laser power values needed to image every sample in the equalization assay. For this, find the most intense sample, as well as the dimmest sample, for each laser line (key samples). Adjust the laser power of each laser line until key samples can be imaged with good quality. Avoid signal saturation or shortage and aim for a range between 20.000 and 30.000 gray values in 16-bit images.
▲ CRITICAL STEP Saturation must be avoided, because it is not quantifiable, and the equalization assay relies on the quantification of the most intense pixels of each image.
? TROUBLESHOOTING

17 Maintaining focus on a fluorescent sample, carefully exchange the sample for the sensor of the laser power meter without changing the stage coordinates.
? TROUBLESHOOTING

18 For each laser line (e.g., 405, 488, 561 and 633 nm) measure and record the output laser power in Watts at the percentage of total laser power chosen in Step 16 (e.g., 3.7–4.2 mW at 0.2% laser power on the 405-nm line). The same wattage will be used for the remaining portion of the assay. Before every equalization replicate, measure and adjust the laser percentages to match the wattage settings of the first round.

19 For each sample, take at least three snapshots of the highest intensity areas in the tissue. Save the snapshots as .czi files.
▲ CRITICAL STEP Marker intensities between equalization-assay replicates are dependent on staining procedure consistency, antibody penetration and imaged tissue area. Pipetting accuracy in the immunostaining and consistency in imaging depth are therefore critical.

Automated marker intensity quantification ● Timing 1 h

▲ CRITICAL To measure signal intensity for each antibody combination, pixels representing positive signal in the images of the equalization assay are identified and quantified. To do this, run the automated STAPL-3D equalization assay analysis pipeline. In the pipeline, the image is segmented first in noise and

tissue regions by smoothing and Otsu thresholding, after which the tissue is divided in foreground (signal of interest) and background through splitting the intensities at quantiles. The resulting metrics include foreground intensity, signal-to-noise ratio and contrast-to-noise ratio. For the analysis in Fig. 2, the foreground intensity was used. Detailed instructions for performing the quantification pipeline are provided at https://github.com/RiosGroup/STAPL3D/blob/master/stapl3d/pipelines/pipeline_equalization.md.

20 Organize imaging files in a directory structure according to:
<*datadir*>/<*species*>/<*antibody*>/<*repetition*>.<*ext*>
Primaries are included as a separate <*species*> in the same data directory:
<*datadir*>/*primaries*/<*antibody*>/<*repetition*>.<*ext*>
▲ **CRITICAL STEP** Ensure that each filename is unique, even if the filenames are in separate directories.

21 Open a terminal, activate the stapl3d conda environment and start the python interpreter.

22 Run the equalization pipeline by issuing the commands:

```
from stapl3d import equalization
equaliz3r = equalization.Equaliz3r('<datadir>')
equaliz3r.run()
```

▲ **CRITICAL STEP** Replace <*datadir*> with the path to the data.

23 Evaluate the rank and score of the antibodies by using the plots and/or csv found in <*datadir*>/*equalization* for their potential position in the panel.
▲ **CRITICAL STEP** We provide a comprehensive STAPL-3D equalization-assay demo including details on the various parameters and options to tailor the analysis to specific needs at https://github.com/RiosGroup/STAPL3D/blob/master/demos/equalization_demo.ipynb.

Procedure 2: general mLSR-3D procedure

▲ **CRITICAL** Apply the appropriate preprocessing and fixation protocol according to your tissue of interest (Box 1). Sample thicknesses in a range of 100–500 µm are recommended for good antibody penetration and reduced processing time. The following procedure is optimized for large and fragile mouse brain slices and therefore relies on well plates for incubation steps. For smaller and denser tissue types, we recommend using 2-ml Eppendorf tubes for antibody incubation steps and 15- or 50-ml tubes for washing. This improves antibody penetration and reduces unwanted background signal.

Blocking ● Timing 4 h

1 Block the tissue in 500 µl of WB1 in a 24-well-plate well and incubate at 4 °C for 4 h on an orbital shaker.
■ **PAUSE POINT** Once blocked, tissue can be stored in WB2 at 4 °C for 2 d or over the weekend. However, fresh tissue performs best, and the protocol should be continued as soon as possible.

Immunolabeling ● Timing 44–66 h

2 Design an eight-color staining mix by using the flow chart in Extended Data Fig. 1 and results from the intensity-equalization assay in Procedure 1. A complete walkthrough example of such a mix design can be found in Box 2.
▲ **CRITICAL STEP** Simultaneous immunostaining of up to eight fluorophores requires careful planning. Antibody cross-reactivity should be avoided. Three rounds of immunostaining are often necessary when combining antibodies raised in different species.
▲ **CRITICAL STEP** Avoid bright and dim combinations in adjacent emission slots.
▲ **CRITICAL STEP** Alternate membranal and nuclear markers when possible.

3 Prepare primary antibody mix by pipetting 500 µl of WB2 in a 1.5-ml Eppendorf, add primary antibodies at the desired concentration (Table 1) and mix well by pipetting up and down several times.

4 Remove WB1 from the well containing the sample and replace with 500 µl of primary antibody mix. Incubate at 4 °C overnight on an orbital shaker.

5 Remove primary antibody mix and wash tissue with 1 ml of WB2 for 1 h at 4 °C on an orbital shaker. Repeat this washing step two additional times for ≥1 h.
▲ **CRITICAL STEP** Careful washing is important to reduce background signal from nonspecific primary antibody binding. Ensure that all the liquid is removed between washing steps and that the tissue is not being damaged during the process.

■ **PAUSE POINT** Once washed, tissue can be stored in WB2 at 4 °C for 2 d or over the weekend. However, fresh tissue performs best, and the protocol should be continued as soon as possible.

6 Prepare secondary antibody mix by pipetting 500 µl of WB2 in a 1.5-ml Eppendorf tube and add secondary antibodies, conjugated primary antibodies and fluorescent dyes at the desired concentration. Mix well by pipetting up and down several times.
▲ **CRITICAL STEP** Do not use the same primary antibody species (e.g., mouse or rabbit) twice, because it will lead to unwanted cross-binding of secondary antibodies. It is possible to use a directly conjugated primary antibody raised in an animal species (e.g., KI67-AF488, rat) that is also the source of another primary antibody in the mix (e.g., CDH1, rat). When this occurs, the antibody labeling can be performed in three rounds: the first round contains the primary CDH1 (rat), the second round contains the secondary anti-rat and the third round contains the conjugated KI67-AF488 (rat).

7 Remove WB2 from the well containing the sample and replace with 500 µl of secondary antibody mix. Incubate at 4 °C overnight on an orbital shaker.

8 Remove secondary antibody mix and wash tissue with 1 ml of WB2 for 1 h at 4 °C on an orbital shaker. Repeat this washing step two additional times for ≥1 h.
▲ **CRITICAL STEP** Keep samples in the dark for all the subsequent steps. Proceed immediately with tissue clearing to avoid any loss of signal.

Tissue clearing using a FUnGI gradient ● Timing 15 h

9 Prepare a dilution of 33% (vol/vol) FUnGI in WB2 and 66% (vol/vol) FUnGI in WB2. Bring FUnGI stock to room temperature for reduced viscosity. Dilute accordingly and homogenize on a roller bank or by vortexing briefly. Keep the required amount of 33%, 66% and 100% (vol/vol) FUnGI solutions at room temperature.
▲ **CRITICAL STEP** Always make fresh FUnGI dilutions on the day of clearing. BSA in the dilutions should not be kept at room temperature for more than 24 h. FUnGI clearing agent is viscous and should be dispensed slowly to avoid bubble formation. Throughout the clearing process the tissue will gradually become translucent and sink to the bottom of the well.

10 Replace WB2 with 1 ml of 33% (vol/vol) FUnGI solution and incubate for 1 h at room temperature with mild rocking or shaking.

11 Carefully remove 33% (vol/vol) FUnGI solution and replace with 66% (vol/vol) FUnGI solution. Incubate for 1 h at room temperature with mild rocking or shaking.

12 Using forceps or a flat spoon, transfer tissue to a new six-well plate with a well containing 2 ml of 100% (vol/vol) FUnGI solution. Incubate at room temperature for 1 h and then overnight at 4 °C with mild rocking or shaking.
▲ **CRITICAL STEP** The FUnGI clearing process is reversible. Samples can be washed with PBT and re-stained or processed differently if required.
■ **PAUSE POINT** Stained and cleared samples can be stored at 4 °C for ≤1 week or at −20 °C for ≤6 months with minimal loss of fluorescent signal.

Sample mounting for mLSR3D imaging ● Timing 30 min

13 Fill a 10-ml syringe with silicon sealant and plug a 200-µl pipette tip on its end. Cut the end of the tip to create an outlet of ~1 mm in diameter. Gently press the syringe until the pipette tip is filled.

14 Place a coverslip on a flat and clean surface and trace a 1 × 2-cm rectangle in the middle by using a fine and homogeneous stream of silicon.

15 Using a flat spoon, forceps or a wide pipette tip, gently transfer the tissue to the center of the rectangle and remove any excess FUnGI solution.

16 Place a second coverslip on top by starting on one side and slowly lowering the coverslip to the other side. This should release any trapped air and ensure homogeneous spreading of FUnGI mounting medium within the delimited rectangle.

17 Seal the tissue by applying light pressure on each side of the coverslip and wait 5 min for the silicon to set. The mounted sample can immediately be used for imaging or stored at 4 °C for ≤1 week or at −20 °C for ≤6 months.
? TROUBLESHOOTING

Multispectral 3D imaging ● Timing dependent on specific tissue

18 Image the tissue (recommended to use a 25× oil-immersion objective) and use the following acquisition settings as a baseline: online fingerprinting mode, activate required spectral reference

signatures (as acquired in Procedure 1, Steps 13 and 14), frame-scanning mode, optical section resolution of 1,024 × 1,024, voxel size of 332 nm × 332 nm × 1.2 µm, pixel dwell time of <2 µs, line step 1, bidirectional scanning, speed of 6, averaging number of 1 and bit depth of 16. Low laser powers are recommended (set to <5% in the microscope software) to reduce photobleaching.

19 Define the lower and upper bounds by using *z*-stack mode, activate tiling mode with an overlap of 10% and select the area of interest.

▲ **CRITICAL STEP** Image acquisition of large 3D tissue through sequential lambda scans can take between several hours and days. Resolution, acquisition speed and *z*-size are some factors influencing this process. File size can be greatly reduced by using microscopy systems equipped with 'on the fly' linear unmixing capabilities as used in mLSR-3D (Supplementary Table 1).

? TROUBLESHOOTING

Image processing ● Timing dependent on file size and computational power specific

▲ **CRITICAL** The STAPL-3D preprocessing pipeline aims to prepare the dataset for accurate quantification. Beyond the basic stitching of the tilescan, corrections are applied to achieve optimal homogeneity over the datasets. This consists of shading correction on the individual z-stacks, as well as 3D inhomogeneity correction on the full dataset after stitching to reduce technical variations in signal intensity. A detailed description of how to perform the STAPL-3D preprocessing pipeline is described in https://github.com/RiosGroup/STAPL3D/blob/master/stapl3d/pipelines/pipeline_preprocessing.md.

20 Organize and name files according to:

<projectdir>/<dataset>/<dataset>.<ext>

21 Open a terminal, activate the stapl3d conda environment and start the python interpreter.

22 Run the shading correction estimation pipeline by issuing the commands:

```
from stapl3d.preprocessing import shading
dataset = '<dataset>'
filepath_raw = f'{dataset}.czi'
steps = ['estimate', 'process', 'postprocess']
deshad3r = shading.Deshad3r(filepath_raw, prefix=dataset)
deshad3r.run(steps)
```

Replace <dataset> with the name of the dataset (without the '.czi' extension).

Shading profile images are calculated for each channel and saved in:

<projectdir>/<dataset>/<dataset> _shading_C<channel>.tif

23 Apply the estimated shading profiles to their respective channel and stich the corrected tile scan by using the Zeiss Zen Blue software. A detailed description of this procedure can be found at https://github.com/RiosGroup/STAPL3D/blob/master/stapl3d/pipelines/pipeline_stitching_zen.md.

- Split raw data into channels.
  Processing > Method > Create Image Subset and Split
- Apply STAPL3D shading profile for each channel.
  Processing > Method > Shading Correction
- Merge the corrected channels back together.
  Processing > Method > Add Channel (iteratively combine sets until all are concatenated)
- Stitch the corrected tilescan in Zeiss Zen software.
  Processing > Method > Stitching
  Save the stitched file as *<projectdir>/<dataset>/<dataset>_shading_stitching.czi*

? TROUBLESHOOTING

24 Convert the stitched czi-file to Imaris v5.5 file format by using the Imaris File Converter software.

25 Run the 3D inhomogeneity correction pipeline by issuing the commands:

```
from stapl3d.preprocessing import biasfield
dataset = '<dataset>'
filepath_stitch = f'{dataset}_shading_stitching.ims'
homogeniz3r = biasfield.Homogeniz3r(filepath_stitch, prefix=dataset)
homogeniz3r.run()
```

The preprocessed data are saved as an Imaris file:
<projectdir>/<dataset>/<dataset>_shading_stitching_biasfield.ims

▲ **CRITICAL STEP** We provide a comprehensive STAPL-3D image preprocessing demo including details on the various parameters and options to tailor the analysis to specific needs at https://github.com/RiosGroup/STAPL3D/blob/master/demos/preprocessing_demo.ipynb.

26 Render the corrected mLSR-3D dataset by using the 3D view tab in the Imaris imaging software and use the display adjustment function to tweak the histograms of all individual channels for optimal representation.

Troubleshooting

Troubleshooting advice can be found in Table 2.

Table 2 | Troubleshooting table

Step	Problem	Possible reason	Solution
Procedure 1, Step 12	Blurry image or the sample cannot be imaged in depth	The FUnGI layer underneath the sample is too thick for the working distance of the objective	Move the tissue to an imaging chamber area with no FUnGI layer or remove excess
Procedure 1, Step 14	The auto-find function cannot discriminate the signal of interest from the background	The signal-to-background ratio is too dim for the auto-find function	Manually select the signal of interest by using the circle tool and click on linear unmixing
Procedure 1, Step 16	Signal saturation on the lowest wattage possible	The antibody or dye concentration is too high and saturates the detector	Exclude the marker from this equalization round and repeat individually with a lower concentration
	A weak marker is not visible with the selected laser power for this laser line	High signal antibody or dye in this laser line is too concentrated and requires very low laser power	Increase the concentration of the low signal marker or decrease the concentration of the high signal marker
Procedure 1, Step 17	Significant changes in wattage compared to the previous equalization experiment	The power meter sensor is not aligned with the laser beam	Activate the brightfield light and move the stage until the light circle aligns with the sensor
Procedure 2, Step 17	The cover glass brakes while applying pressure	The silicon layer is uneven or too thick	Reduce the diameter of the pipette tip while applying the silicon line
	Bubbles are introduced on top of the sample during mounting	The FUnGI solution contains bubbles before mounting, or trapped air was not pushed out during mounting	Move the sample to a new FUnGI solution without bubbles or manually remove them by using a pipette
Procedure 2, Step 19	The sample is drifting away from the objective during acquisition	The sample is trapped between two layers of FUnGI solution during mounting and is not secured in place. The objective is applying pressure on the coverslip and squeezing it to the side	Reduce the amount of FUnGI solution during mounting and ensure that the objective has a sufficient working distance to never touch the cover glass
	Saturating signal in areas of the tissue	Impurities in the FUnGI solution or on top of the tissue	Wash the tissue thoroughly after each immunostaining step and ensure that no impurities are introduced
Procedure 2, Step 23	Stitching of imaging files takes too long or crashes	The workstation is not equipped with enough RAM (random access memory) to process the dataset	Upgrade the computer RAM or limit dataset size to the maximum file size possible to be processed with this hardware. Alternatively, move to a high-performance computing cluster

Timing

Procedure 1: equalization assay

Steps 1–2, sample dissection and blocking: 6 h
Steps 3–8, high-throughput single-staining: 44 h
Steps 9–12, tissue clearing using a FUnGI gradient: 15 h
Steps 13–14, spectral signature reference library acquisition: 2 h
Steps 15–19, imaging for intensity-equalization assay: 4–5 h
Steps 20–23, automated marker intensity quantification: 1 h

Procedure 2: general mLSR-3D procedure

Step 1, tissue blocking: 4 h
Steps 2–8, mix design and immunolabeling: 44–66 h
Steps 9–12, tissue clearing using a FUnGI gradient: 15 h
Steps 13–17, sample mounting for mLSR3D imaging: 30 min
Steps 18–19, multispectral 3D imaging: 1–24 h, depending on tissue size
Steps 20–26, image processing: 1–48 h, depending on file size and computational power

Anticipated results

In this protocol, we describe a reproducible and structured approach for achieving eight-color 3D imaging data with mLSR-3D. The equalization assay provides, in a single overview, the relative intensities for all required antibodies and dyes (Fig. 2,b). Although this assay requires investment of time and resources initially, in our experience, it is more efficient than a trial-and-error immunolabeling approach. The results of the equalization assay guide the selection of appropriate antibody and dye combinations that can be visualized together by the same laser. As an example, we show equalization of the 488- and 633-nm laser lines (Fig. 2c). For the 488-nm laser, the neuronal marker NeuN can be combined with anti-rabbit-AF514 to match the intensity of Phalloidin-AF488. Similarly, NCAD together with anti-sheep-AF633 has equal emission intensity as KI67-eFluor660. We combine this with FUnGI, which renders samples of various composition transparent for 3D imaging, demonstrated here on human healthy and Wilms tumor epithelial kidney tissue and a mouse brain specimen (Fig. 2d). For optimal fast clearing, short stepwise incubations of 1 h in diluted FUnGI solution with increasing concentrations, followed by an overnight incubation with 100% FUnGI solution (as detailed in our protocol) was observed to work best. However, the penetration depth of

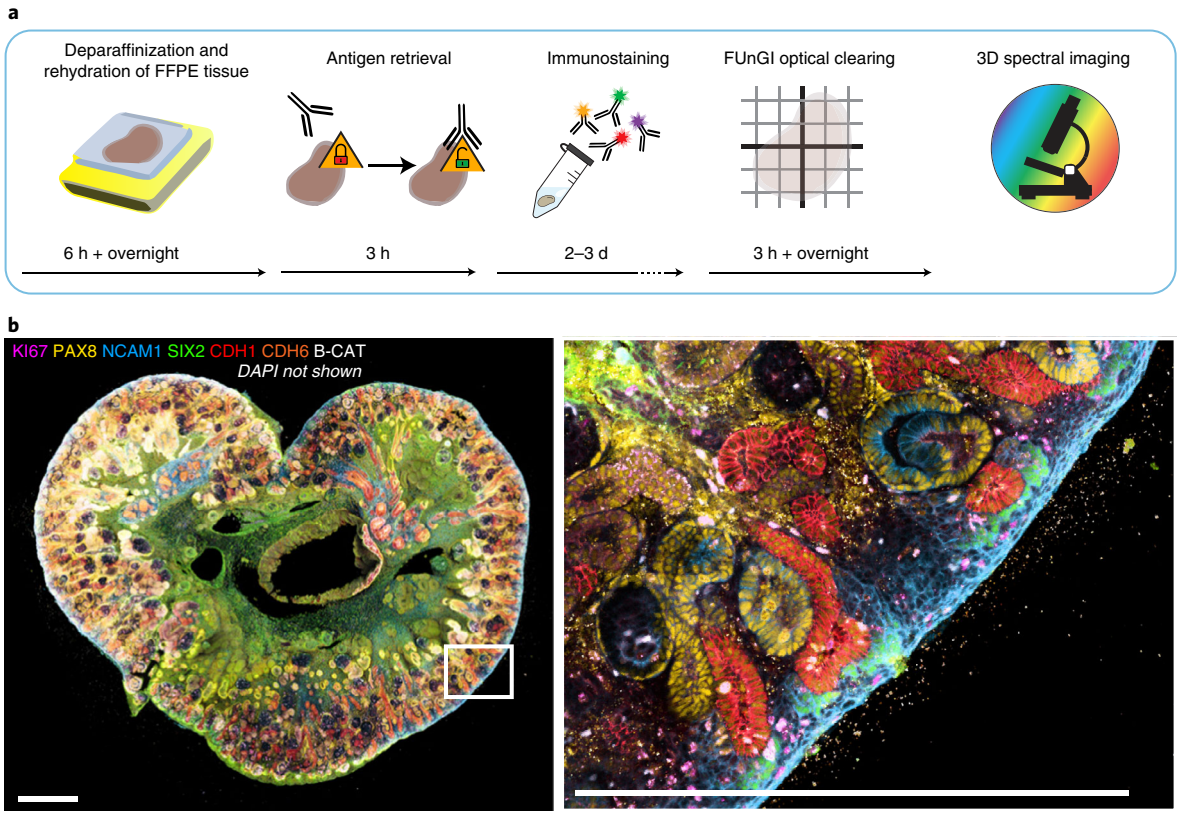

Fig. 5 | mLSR-3D imaging of deparaffinized FFPE tissue. a, Schematic overview of the mLSR-3D protocol for intact FFPE tissue blocks. After sample deparaffinization, rehydration and antigen retrieval, eight-marker immunostaining and optical clearing with FUnGI are performed per the standard mLSR-3D procedure. **b**, 3D rendering of human fetal kidney (15 weeks of gestation) labeled for DAPI (not shown), KI67 (magenta), PAX8 (yellow), NCAM1 (blue), SIX2 (green), CDH1 (red), CDH6 (orange) and B-CAT (white). Scale bars, 500 µm. Overview image (left) and magnification of indicated area (white square) (right).

Fig. 6 | mLSR-3D guided comparative spatio-phenotypic analysis of human brain tumors. a, 3D rendering of malignant glioma of the frontal lobe (high-grade glioma) labeled for DAPI (gray), F-ACTIN (signal intensity gradient: red-yellow-white), OLIG2 (magenta), KI67 (green), SMA (yellow), IBA1 (blue) and MAP2 (cyan). Scale bars, 500 μm (overview) and 100 μm (magnification). **b**, 3D representation of pilocytic astrocytoma of the occipital lobe (low-grade glioma) labeled for DAPI (gray), F-ACTIN (signal intensity gradient: red-yellow-white), OLIG2 (magenta), TUBB3 (yellow), KI67 (green), GFAP (red), IBA1 (blue) and MAP2 (cyan). Scale bars, 500 μm (overview) and 100 μm (magnification). **c** and **d**, Optical sections depicting DAPI (left), nuclear segmentation (middle) and volume feature backprojection (right) for high-grade glioma (**c**) and low-grade glioma (**d**). Scale bars, 50 μm. **e**, The color gradient represents volume in voxels. Violin and boxplots showing difference in nuclear volume in voxels between the tumors. Center: median; bounds: Q1–Q3; whiskers extend to minimum/maximum limited to 1.5 times the interquartile range. Mann–Whitney U test; ***, $P < 2.22 \times 10^{16}$. **f**, Violin and boxplots showing *z*-score–normalized mean values for KI67 intensity plotted on a logarithmic y-axis. Center: median; bounds: Q1–Q3; whiskers extend to minimum/maximum limited to 1.5 times the interquartile range. The red dashed line indicates the threshold for KI67 positivity at 0.916, which corresponds to a log *z*-score of 2.5. **g**, Quantification of KI67 positivity per tumor visualized in 100% stacked bar plots. Pearson's chi-squared test with Yates' continuity correction; ***, $P < 2.2 \times 10^{16}$.

FUnGI can be expanded by longer incubations. Excellent preservation of tissue structure and compatibility with both native and immunofluorescence result in large 3D imaging datasets with high signal quality.

Here, we demonstrate 3D-rendered datasets of human fetal kidney at gestational week 12 (Fig. 3a and Supplementary Movie 1), pediatric kidney Wilms tumor (Fig. 3b), xenografted breast cancer organoids (Fig. 3c and Supplementary Movie 1) and breast cancer organoids in culture (Fig. 3d). The high number of fluorescent markers obtained gives better context for spatio-phenotypic patterning and phenotypic characterization, as demonstrated previously[26]. In addition, mLSR-3D can also be used to specifically unmix autofluorescent structures, such as blood vessels in mouse brain (Fig. 4a), combined with the visualization of fine cellular structures of GFAP positive astrocytes at the glio-vascular interface (Fig. 4b). The excellent retention of native fluorescence by mLSR-3D allows the visualization of patient-derived DMG cells expressing mNeonGreen, together with the immunostained markers (Fig. 4a). This enables the evaluation of tumor cell migration trajectory from a primary engraftment site in the pontine area toward the medulla and cerebellum in this xenograft model. Another tumor cell migration model is demonstrated by a cerebral organoid[46] fused with a patient-derived DMG organoid (Fig. 4c). In this model, tumor cells can be identified distant from the fusion site, confirming cell migration. mLSR-3D is uniquely suited to evaluate these tumor migration models, because large volumes must be imaged, while at the same time resolving fine-detailed structures and single cells. In addition, multispectral imaging aids in providing tissue context and reducing autofluorescent artefacts. Although mLSR-3D is optimized for confocal microscopy, it is directly compatible with two-photon excitation. We exemplify this with a pediatric kidney Wilms tumor sample labeled with six colors and recorded in a single acquisition with spectral imaging and linear unmixing using two-photon excitation (Extended Data Fig. 4). This approach might extend the achievable imaging depth and illustrates the broader applicability of our protocol.

With minor adaptations to the protocol (detailed in Box 3), FUnGI optical clearing (Fig. 2d) and mLSR-3D are compatible with FFPE samples, and we demonstrate single-cell-resolution 3D imaging data from deparaffinized FFPE human fetal kidney at gestational week 15 (Fig. 5). However, as expected, deparaffinized samples show more tissue deformation artefacts as compared to PFA-fixed samples. These deformation artefacts are caused by shrinkage and expansion of the tissue because of de- and rehydration procedures. In our hands, these seemed to have limited effect on cell morphology (Fig. 5b) but could introduce gaps and separation of connective and epithelial tissue, as also commonly seen in histopathological images[47]. In addition to this, we observed more tissue autofluorescence throughout the visible spectrum (data not shown). Importantly, mLSR-3D can specifically unmix this tissue autofluorescence from the other channels if a spectral reference for it has been recorded. mLSR-3D imaging of FFPE material will not only be of interest to preclinical researchers, but also to clinicians and pathologists and can open up a wealth of tissue information stored in patient sample biobanks[48]. As such, 3D imaging of FFPE samples with availability of relevant clinical information, including diagnosis and patient outcome, would allow for correlative and predictive analyses and could be used to validate new biomarkers for diagnosis and treatment response.

The single-cell resolution that is obtained by mLSR-3D can be exploited for single-cell analysis. Using STAPL-3D[26], we performed a comparative analysis between a low-grade (pilocytic astrocytoma) and high-grade (frontal lobe) human brain tumor by segmenting 285,000 and 190,000 nuclei, respectively (Fig. 6a–d and Supplementary Movie 1). The cell nuclei in the low-grade glioma were significantly larger than those in the high-grade glioma, as can be seen from the quantified nuclear volumes (Fig. 6e). In addition, for both samples, we assessed the KI67 index (Fig. 6f), used in

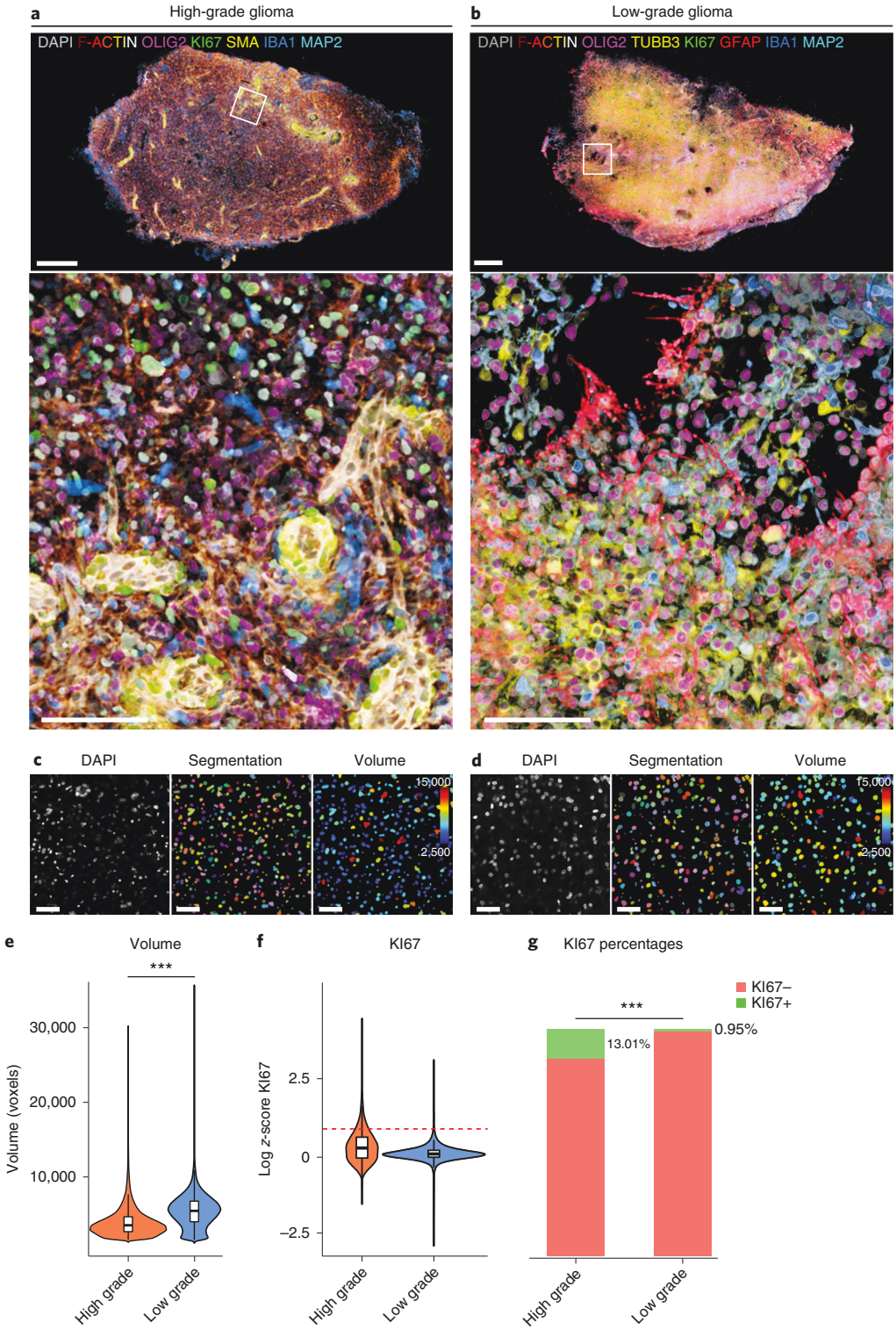

oncology to ascertain proliferation status and often correlating with tumor aggressiveness. As expected, low-grade glioma displayed a lower KI67 index (0.95%) than did high-grade glioma (13.01%), reflecting its characteristic slow growth (Fig. 6g)[49,50]. Although we here demonstrate an impact for cancer research, given the versatility of our approach, utility reaches beyond oncology and includes neuroscience and developmental biology, as shown by mLSR-3D imaging of mouse brain tissue (Fig. 4a,b) and fetal kidney (Figs. 3a and 5b).

Data availability

All data described in this protocol are available from the corresponding author upon reasonable request. Representative subsetted datasets and analyses are made publicly available through demos on the STAPL-3D GitHub page (https://github.com/RiosGroup/STAPL3D).

Code availability

All source codes of STAPL-3D are publicly available through GitHub (https://github.com/RiosGroup/STAPL3D).

References

1. Belle, M. et al. Tridimensional visualization and analysis of early human development. *Cell* **169**, 161–173.e12 (2017).
2. Hannezo, E. et al. A unifying theory of branching morphogenesis. *Cell* **171**, 242–255.e27 (2017).
3. Rios, A. C., Fu, N. Y., Lindeman, G. J. & Visvader, J. E. In situ identification of bipotent stem cells in the mammary gland. *Nature* **506**, 322–327 (2014).
4. Scheele, C. L. G. J. et al. Identity and dynamics of mammary stem cells during branching morphogenesis. *Nature* **542**, 313–317 (2017).
5. Murakami, T. C. et al. A three-dimensional single-cell-resolution whole-brain atlas using CUBIC-X expansion microscopy and tissue clearing. *Nat. Neurosci.* **21**, 625–637 (2018).
6. Messal, H. A. et al. Tissue curvature and apicobasal mechanical tension imbalance instruct cancer morphogenesis. *Nature* **566**, 126–130 (2019).
7. Rios, A. C. et al. Intraclonal plasticity in mammary tumors revealed through large-scale single-cell resolution 3D imaging. *Cancer Cell* **35**, 953 (2019).
8. Brown, M. et al. Lymph node blood vessels provide exit routes for metastatic tumor cell dissemination in mice. *Science* **359**, 1408–1411 (2018).
9. Almagro, J., Messal, H. A., Thin, M. Z., van Rheenen, J. & Behrens, A. Tissue clearing to examine tumour complexity in three dimensions. *Nat. Rev. Cancer* **21**, 718–730 (2021).
10. Ertürk, A. et al. Three-dimensional imaging of solvent-cleared organs using 3DISCO. *Nat. Protoc.* **7**, 1983–1995 (2012).
11. Messal, H. A. et al. Antigen retrieval and clearing for whole-organ immunofluorescence by FLASH. *Nat. Protoc.* **16**, 239–262 (2021).
12. Dekkers, J. F. et al. High-resolution 3D imaging of fixed and cleared organoids. *Nat. Protoc.* **14**, 1756–1771 (2019).
13. Bernier-Latmani, J. & Petrova, T. V. High-resolution 3D analysis of mouse small-intestinal stroma. *Nat. Protoc.* **11**, 1617–1629 (2016).
14. Kusumbe, A. P., Ramasamy, S. K., Starsichova, A. & Adams, R. H. Sample preparation for high-resolution 3D confocal imaging of mouse skeletal tissue. *Nat. Protoc.* **10**, 1904–1914 (2015).
15. Susaki, E. A. et al. Advanced CUBIC protocols for whole-brain and whole-body clearing and imaging. *Nat. Protoc.* **10**, 1709–1727 (2015).
16. Tomer, R., Ye, L., Hsueh, B. & Deisseroth, K. Advanced CLARITY for rapid and high-resolution imaging of intact tissues. *Nat. Protoc.* **9**, 1682–1697 (2014).
17. Renier, N. et al. iDISCO: a simple, rapid method to immunolabel large tissue samples for volume imaging. *Cell* **159**, 896–910 (2014).
18. Susaki, E. A. & Ueda, H. R. Whole-body and whole-organ clearing and imaging techniques with single-cell resolution: toward organism-level systems biology in mammals. *Cell Chem. Biol.* **23**, 137–157 (2016).
19. Tainaka, K., Kuno, A., Kubota, S. I., Murakami, T. & Ueda, H. R. Chemical principles in tissue clearing and staining protocols for whole-body cell profiling. *Annu. Rev. Cell Dev. Biol.* **32**, 713–741 (2016).
20. Richardson, D. S. & Lichtman, J. W. Clarifying tissue clearing. *Cell* **162**, 246–257 (2015).
21. Li, W., Germain, R. N. & Gerner, M. Y. High-dimensional cell-level analysis of tissues with Ce3D multiplex volume imaging. *Nat. Protoc.* **14**, 1708–1733 (2019).
22. Ku, T. et al. Elasticizing tissues for reversible shape transformation and accelerated molecular labeling. *Nat. Methods* **17**, 609–613 (2020).
23. Goltsev, Y. et al. Deep profiling of mouse splenic architecture with CODEX multiplexed imaging. *Cell* **174**, 968–981.e15 (2018).
24. Seo, J. et al. PICASSO allows ultra-multiplexed fluorescence imaging of spatially overlapping proteins without reference spectra measurements. *Nat. Commun.* **13**, 2475 (2022).
25. Murray, E. et al. Simple, scalable proteomic imaging for high-dimensional profiling of intact systems. *Cell* **163**, 1500–1514 (2015).
26. van Ineveld, R. L. et al. Revealing the spatio-phenotypic patterning of cells in healthy and tumor tissues with mLSR-3D and STAPL-3D. *Nat. Biotechnol.* **39**, 1239–1245 (2021).
27. Stoltzfus, C. R. et al. CytoMAP: a spatial analysis toolbox reveals features of myeloid cell organization in lymphoid tissues. *Cell Rep.* **31**, 107523 (2020).
28. Wang, X. et al. Three-dimensional intact-tissue sequencing of single-cell transcriptional states. *Science* **361**, eaat5691 (2018).

29. Alon, S. et al. Expansion sequencing: spatially precise in situ transcriptomics in intact biological systems. *Science* **371**, eaax2656 (2021).
30. Valm, A. M. et al. Applying systems-level spectral imaging and analysis to reveal the organelle interactome. *Nature* **546**, 162–167 (2017).
31. Coutu, D. L., Kokkaliaris, K. D., Kunz, L. & Schroeder, T. Multicolor quantitative confocal imaging cytometry. *Nat. Methods* **15**, 39–46 (2018).
32. Zimmermann, T., Marrison, J., Hogg, K. & O'Toole, P. Confocal microscopy, methods and protocols. *Methods Mol. Biol.* **1075**, 129–148 (2013).
33. Susaki, E. A. et al. Whole-brain imaging with single-cell resolution using chemical cocktails and computational analysis. *Cell* **157**, 726–739 (2014).
34. Weiss, K. R., Voigt, F. F., Shepherd, D. P. & Huisken, J. Tutorial: practical considerations for tissue clearing and imaging. *Nat. Protoc.* **16**, 2732–2748 (2021).
35. Gerner, M. Y., Kastenmuller, W., Ifrim, I., Kabat, J. & Germain, R. N. Histo-cytometry: a method for highly multiplex quantitative tissue imaging analysis applied to dendritic cell subset microanatomy in lymph nodes. *Immunity* **37**, 364–376 (2012).
36. Gehart, H. et al. Identification of enteroendocrine regulators by real-time single-cell differentiation mapping. *Cell* **176**, 1158–1173.e16 (2019).
37. van Ineveld, R. L., Ariese, H. C. R., Wehrens, E. J., Dekkers, J. F. & Rios, A. C. Single-cell resolution three-dimensional imaging of intact organoids. *J. Vis. Exp.* **2020**, e60709 (2020).
38. Calandrini, C. et al. An organoid biobank for childhood kidney cancers that captures disease and tissue heterogeneity. *Nat. Commun.* **11**, 1310 (2020).
39. Hu, H. et al. Long-term expansion of functional mouse and human hepatocytes as 3D organoids. *Cell* **175**, 1591–1606.e19 (2018).
40. Post, Y. et al. Snake venom gland organoids. *Cell* **180**, 233–247.e21 (2020).
41. Schutgens, F. et al. Tubuloids derived from human adult kidney and urine for personalized disease modeling. *Nat. Biotechnol.* **37**, 303–313 (2019).
42. Lee, S. S.-Y., Bindokas, V. P. & Kron, S. J. Multiplex three-dimensional optical mapping of tumor immune microenvironment. *Sci. Rep.* **7**, 17031 (2017).
43. Jahr, W., Schmid, B., Schmied, C., Fahrbach, F. O. & Huisken, J. Hyperspectral light sheet microscopy. *Nat. Commun.* **6**, 7990 (2015).
44. Cutrale, F. et al. Hyperspectral phasor analysis enables multiplexed 5D in vivo imaging. *Nat. Methods* **14**, 149–152 (2017).
45. Thomson, J. A. et al. Embryonic stem cell lines derived from human blastocysts. *Science* **282**, 1145–1147 (1998).
46. Lancaster, M. A. & Knoblich, J. A. Generation of cerebral organoids from human pluripotent stem cells. *Nat. Protoc.* **9**, 2329–2340 (2014).
47. Taqi, S. A., Sami, S. A., Sami, L. B. & Zaki, S. A. A review of artifacts in histopathology. *J. Oral. Maxillofac. Pathol. Jomfp* **22**, 279–279 (2018).
48. Kokkat, T. J., Patel, M. S., McGarvey, D., LiVolsi, V. A. & Baloch, Z. W. Archived formalin-fixed paraffin-embedded (FFPE) blocks: a valuable underexploited resource for extraction of DNA, RNA, and protein. *Biopreserv. Biobank.* **11**, 101–106 (2013).
49. Wong, E. et al. Cut-point for Ki-67 proliferation index as a prognostic marker for glioblastoma. *Asia Pac. J. Clin. Oncol.* **15**, 5–9 (2019).
50. Tavares, C. B., Braga, F. D. C. S. A. G., Sousa, E. B. & de O. Brito, J. N. P. Expression of Ki-67 in low-grade and high-grade astrocytomas. *–J. Bras. Neurocirur.* **27**, 225–230 (2018).

Acknowledgements

This project has received funding from the European Research Council (ERC) under the European Union's Horizon 2020 research and innovation programme (grant agreement no. 804412). This work was also financially supported by the Princess Máxima Center for Pediatric Oncology and a St. Baldrick's Robert J. Arceci International Innovation award to A.C.R.

Author contributions

R.L.v.I. conceived the protocol. R.L.v.I., R.C., M.B.R. and H.C.R.A. performed experiments and analyzed data. A.P. performed FFPE tissue experiments. N.B. and H.C.R.A. performed brain organoid culturing and imaging. M. Kool provided hESC. M. Kleinnijenhuis designed STAPL-3D and performed data analyses. S.M.C.d.S.L. provided human fetal kidney material. M.B.R. made the video. A.C.R. helped design the protocol. R.L.v.I. and R.C. wrote the manuscript. M.B.R., M.A., E.J.W. and A.C.R. co-wrote the manuscript. A.C.R. supervised the project.

Competing interests

The authors declare no competing interests.

Additional information

Extended data is available for this paper at https://doi.org/10.1038/s41596-022-00739-x.

Supplementary information The online version contains supplementary material available at https://doi.org/10.1038/s41596-022-00739-x.

Correspondence and requests for materials should be addressed to Anne C. Rios.

Peer review information *Nature Protocols* thanks Irene Costantini and the other, anonymous, reviewer(s) for their contribution to the peer review of this work.

Received: 6 October 2021; Accepted: 16 June 2022;
Published online: 30 September 2022

Related links
Key reference using this protocol
van Ineveld, R. L. et al. *Nat. Biotechnol.* **39**, 1239–1245 (2021): https://doi.org/10.1038/s41587-021-00926-3

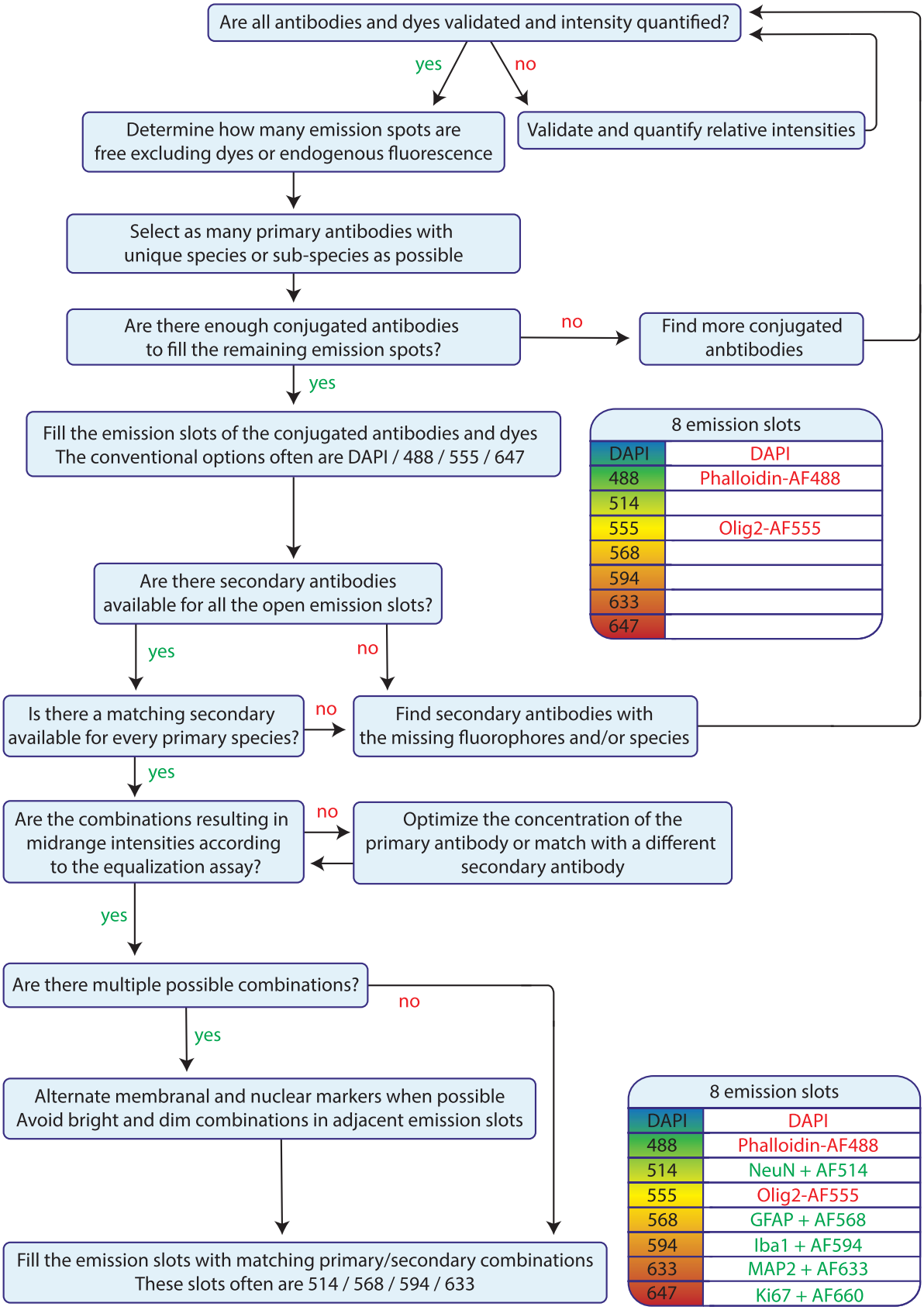

Extended Data Fig. 1 | Workflow for spectral eight-color mix design with commercially available antibodies. Emission slot tables serve as an example for marker mix design and present one possible combination of dyes and antibodies specific to brain tissue.

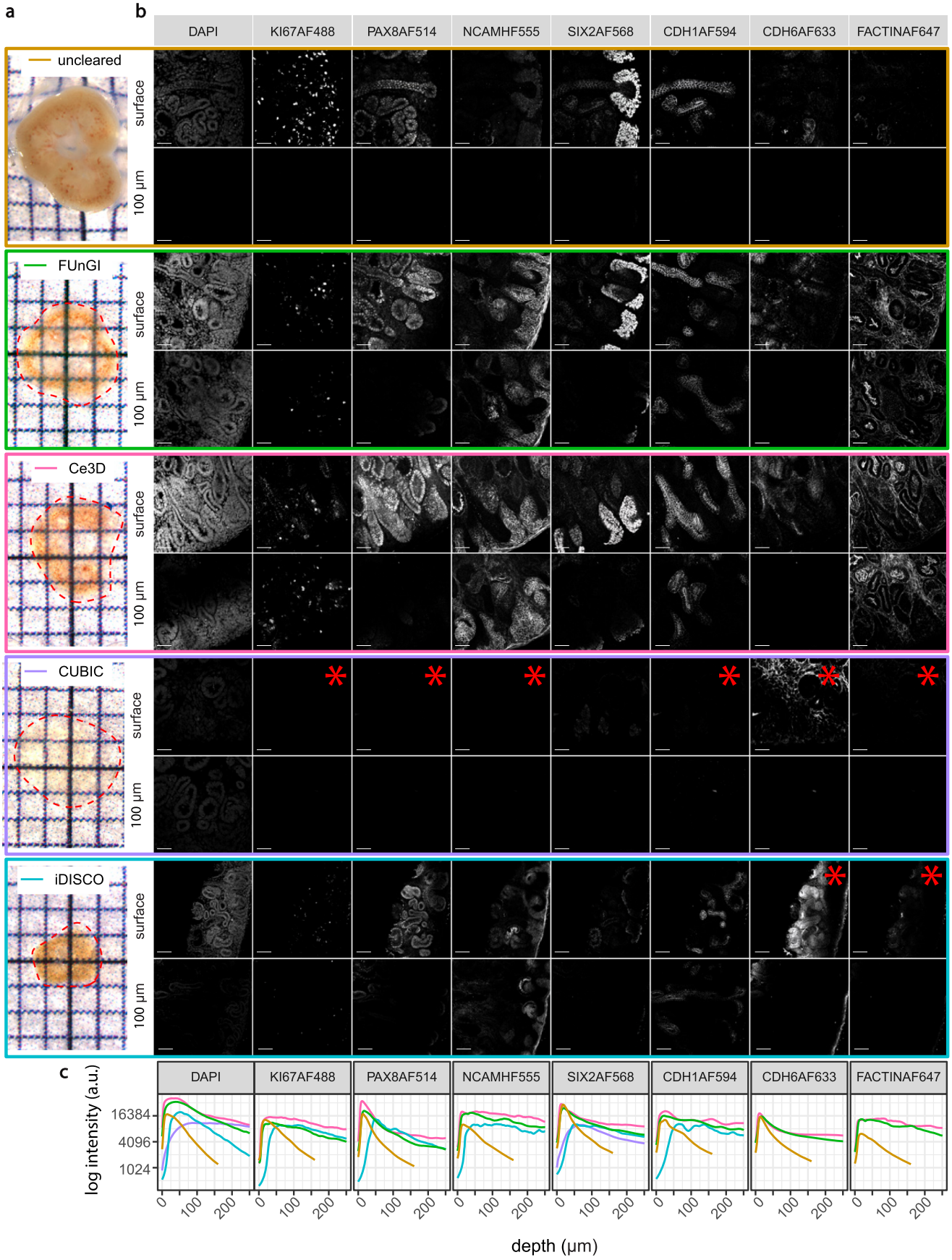

Extended Data Fig. 2 | See next page for caption.

Extended Data Fig. 2 | Clearing comparison. a, Widefield microscopic images of human embryonic kidney tissues uncleared or cleared with FUnGI, Ce3D, CUBIC or iDISCO. Squares represent 1 mm. **b**, Optical sections at two depths (surface and 100 μm) for all eight channels per condition. Red asterisks indicate lack of specific signal in this channel. Scale bars, 50 μm. **c**, Quantification of the 10% highest intensity pixels per *z*-plane per channel for every condition. Channels without sufficient specific signal indicated with a red asterisk were not quantified.

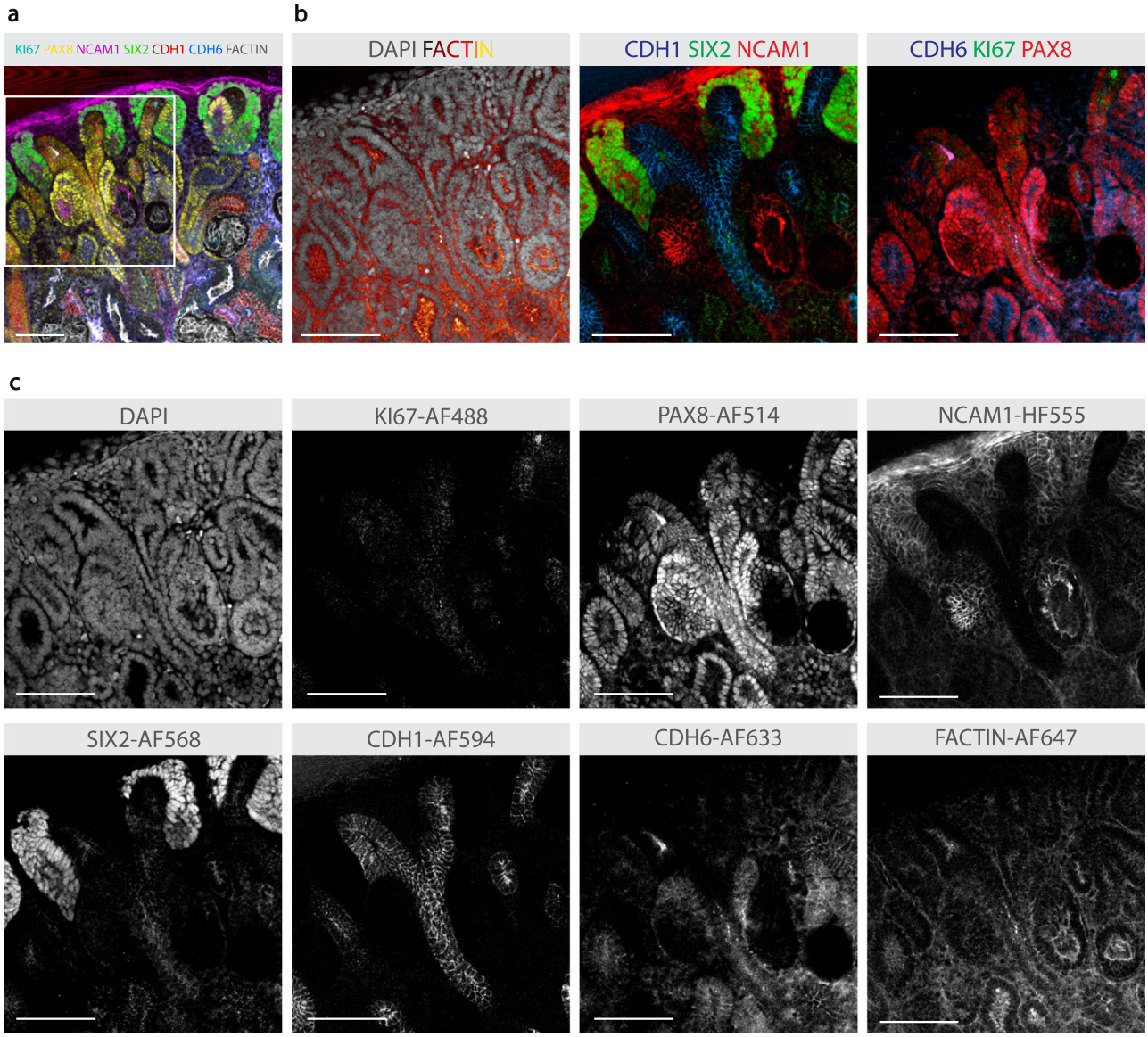

Extended Data Fig. 3 | Sequential 32-channel lambda-scan performed on a Leica SP8. a, Optical section of unmixed eight-color labeled human embryonic kidney. DAPI (not shown), KI67 (aqua), PAX8 (yellow), NCAM1 (magenta), SIX2 (green), CDH1 (red), CDH6 blue) and F-ACTIN (gray). Scale bar, 50 μm. **b**, Magnification of white inset of **a** depicting optical sections of combinations of overlay channels for visual inspection. DAPI (gray), F-ACTIN (signal intensity gradient: red-yellow-white) (left), CDH1 (blue), SIX2 (green), NCAM1 (red) (middle), CDH6 (blue), KI67 (green), PAX8 (red) (right). Scale bars, 50 μm. **c**, Single-channel optical sections of the white inset in **a** for visual inspection. Scale bars, 50 μm.

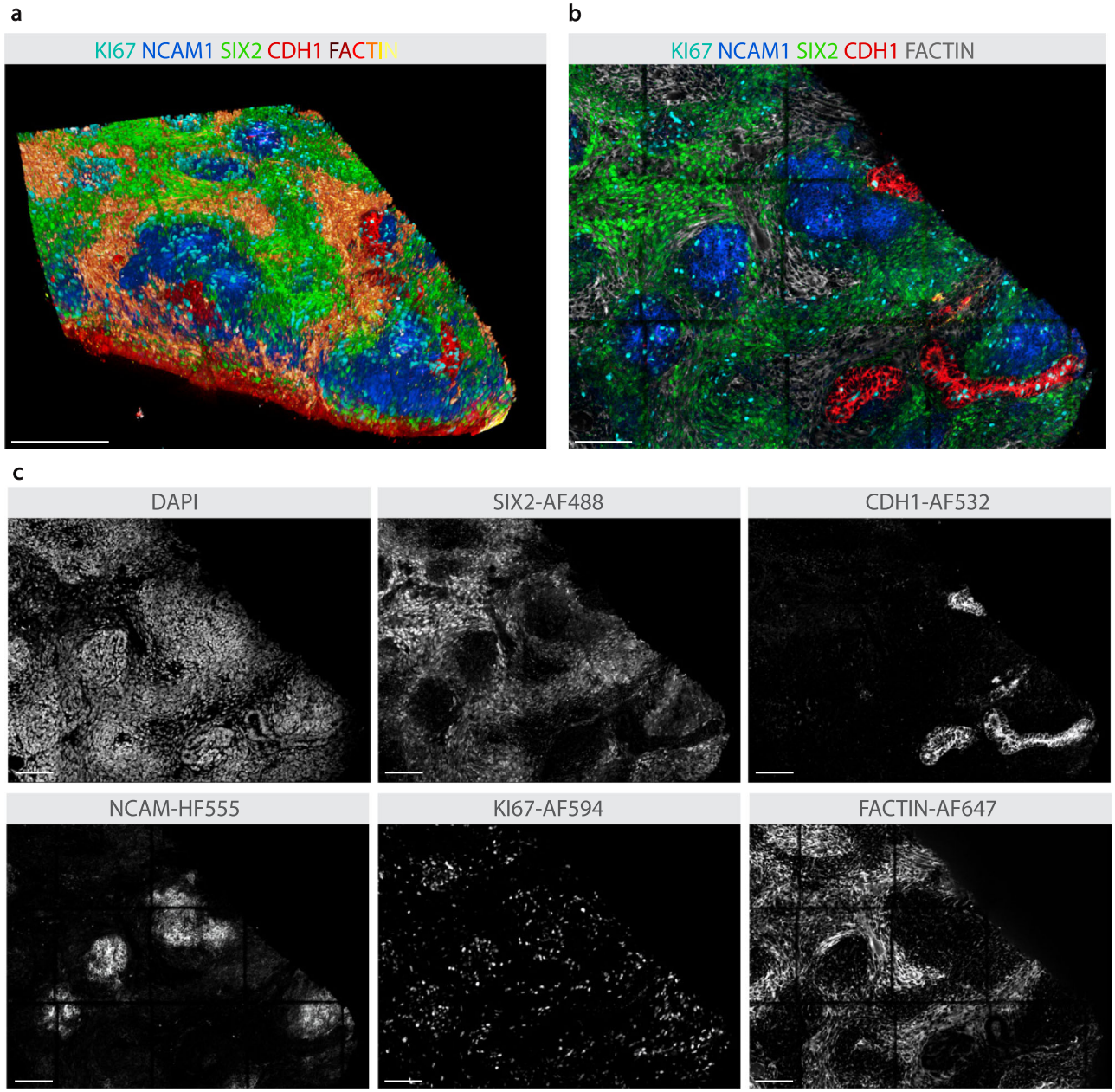

Extended Data Fig. 4 | Two-photon six-color spectral imaging. a, 3D rendering of a human pediatric Wilms tumor sample labeled with DAPI (not shown), KI67 (cyan), NCAM1 (blue), SIX2 (green), CDH1 (red) and F-ACTIN (signal intensity gradient: black-red-orange-yellow). **b**, Wilms tumor dataset labeled with DAPI (not shown), KI67 (cyan), NCAM1 (blue), SIX2 (green), CDH1 (red) and F-ACTIN (gray). Scale bar, 100 μm. **c**, Single-channel optical sections of the same Wilms tumor dataset. Scale bars, 100 μm.